Direct numerical simulations of flameless combustion

Doan, N. A.K.

DOI
10.1016/B978-0-323-85244-9.00002-2

Publication date
2022

Document Version
Final published version

Published in
Fundamentals of Low Emission Flameless Combustion and Its Applications

CHAPTER

8

Direct numerical simulations of flameless combustion

N.A.K. Doan

Faculty of Aerospace Engineering, Delft University of Technology, Delft, The Netherlands

OUTLINE

Abbreviations

CEM Chemical explosive mode
CEMA Chemical explosive mode analysis

Fundamentals of Low Emission Flameless Combustion and Its Applications
https://doi.org/10.1016/B978-0-323-85244-9.00002-2

CV	Controlling variable
DNN	Deep feedforward neural network
DNS	Direct numerical simulation
EGR	Exhaust gas recirculation
FGM	Flamelet-generated manifold
HCCI	Homogeneous charge compression ignition
IML	Igniting mixing layer
JHC	Jet in hot coflow
JSD	Jansen-Shannon divergence
LES	Large eddy simulation
MILD	Moderate or intense low-oxygen dilution
PaSR	Partially stirred reactor
PDF	Probability density function
PLIF	Planar laser-induced fluorescence
PSR	Perfectly stirred reactor
RANS	Reynolds averaged Navier-Stokes
SCCI	Stratified charge compression ignition

1 Introduction

Moderate or intense low-oxygen dilution (MILD) combustion, also called flameless combustion, has been identified as a promising candidate to drastically reduce the pollutant emissions of combustion-based energy-conversion devices [1–4]. In past studies [2, 5–7], these improvements have been demonstrated in experiments, where significant reductions in noise and pollutant emissions, as well as an increase in energy efficiency, were observed. MILD combustion is defined as a combustion process, where the reactants are preheated at a temperature T_r which is higher than the mixture autoignition temperature, T_{ign}, and where the maximum temperature rise, $\Delta T = T_p - T_r$, is smaller than T_{ign}, with T_p being the products temperature [3]. The limited increase in temperature during the combustion process is achieved thanks to the high dilution of the reactants with products and the low level of oxygen available for the combustion. The combustion is, however, maintained and stabilized by the high reactants temperature and the presence of recirculating radicals [1–3, 7].

Since those seminal works, additional research has endeavored to understand the physical mechanisms driving those attractive qualities of MILD combustion. In particular, various experiments have provided several insights as well as competing views on the physical process underpinning MILD combustion [4, 6, 8, 9]. As its name indicates, MILD/flameless combustion occurs with the apparent absence of a visible flame, which made any observation difficult. As a result, advanced laser diagnostics have been carried out to measure the species and temperature distributions in flameless combustion in furnace-type burners, where internal exhaust gas recirculation is present [6, 7, 10]. In those experiments, distributed reaction zones with homogeneous temperature fields and large OH reaction zone were observed. This contrasted MILD combustion from

conventional combustion where reaction zones are generally restricted to thin regions. Subsequent experimental studies focused on simplified configurations without internal exhaust gas recirculation called the jet in hot coflow (JHC), where a high momentum central fuel jet issues into a coflow of air mixed with combustion products, thereby achieving MILD combustion conditions [8, 9, 11]. The hot products, in this case, came from a secondary burner at an upstream position. Using this configuration, experiments could focus on analyzing the effects of this fuel/hot-diluted oxidizer interactions and provide some insights into the physics of MILD combustion with, sometimes, contrasting observations regarding the structure of reaction zones and their combustion mode. For example, the identification of reaction zones using CH_2O planar laser-induced fluorescence (PLIF) showed the existence of distributed reaction zones [9, 12], which was in agreement with an earlier observation from OH-PLIF in a MILD combustion furnace configuration [6]. However, the presence of thin reaction zones was also observed from OH-PLIF performed on the JHC [9, 12] thereby suggesting that there may be a coexistence between distributed and thin reaction zones in MILD combustion.

In addition, another aspect of MILD combustion which is subject to contrasting observations is the combustion mode driving MILD combustion and the relative importance of autoignition versus deflagration. Early experiments using direct photographs or laser thermometry to identify features of MILD combustion [6, 7, 13] showed spatially uniform combustion without a clearly visible flame. However, more advanced techniques like OH-PLIF have shown the existence of thin zones with clear OH gradient [9, 12, 14] suggesting the existence of flame fronts and deflagrative structures. However, autoignition is likely to also play a major role given that $T_r > T_{ign}$ [2, 3, 5]. This autoignition process was studied in the JHC configuration using CH_2O-PLIF [12, 15] and it was observed that the heated coflow played a key role in sustaining the combustion by initiating ignition after localized extinction caused by entrainment of the surrounding cold air. Despite this interplay between extinction and ignition, the abundance of exhaust gas ensured sustained combustion. Oldenhof et al. [11] further analyzed the evolution of these ignition kernels using UV luminescence and observed that ignition kernels were constantly produced and grew in size as they were convected downstream. Similar observations were reported in a jet in hot crossflow [14]. The importance of autoignition appearing at the most reactive mixture fraction, Z_{MR}, was noted in Abtahizadeh et al. [16] at the flame base. These kernels then propagated toward a stoichiometric and richer mixture. These various experimental observations suggested a powerful interplay between autoignition and flame propagation in MILD combustion [3, 17] whose balance needs to be investigated further to improve our understanding of this combustion, especially as this will have a large impact on the modeling of MILD combustion. The modeling approach should, indeed,

be able to capture both autoignition and flame-propagation phenomena and appropriately balance them.

The contrasting views outlined above on the physics of MILD combustion illustrate the need to supplement MILD combustion experimental research with ways to more finely analyze the physics of MILD combustion. This knowledge can be provided with numerical simulations thanks to the recent increase in computational power. Among the various simulation paradigms, direct numerical simulations (DNS) are best suited to provide such fundamental physical insights. Indeed, compared to other simulation approaches, such as Reynolds averaged Navier-Stokes (RANS) simulation or large eddy simulation (LES), DNS does not require any modeling assumption and can thus give the necessary insights into the fundamental physics of MILD combustion. As such, DNS has played a crucial role in developing our understanding of MILD combustion by providing the basis for the development of appropriate modeling frameworks for MILD combustion.

The objective of this chapter was to summarize the findings obtained from such works that relied on DNS of MILD combustion to study its underlying physics. In particular, the focus here was on the results that discussed the inception of MILD combustion, the competition between the various combustion modes (autoignition/deflagration), and the impact of those results on the development of adequate RANS/LES models for MILD combustion as well as past assessments of modeling frameworks for MILD combustion using DNS. This chapter is organized in the following manner. Section 2 describes how the various DNS of MILD combustion were conducted and presents their particularities and turbulent and thermochemical conditions. Section 3 discusses the physical insights obtained from those DNS with a focus on the inception of MILD combustion, the balance between deflagration, and ignition phenomena. Section 4 presents various works that used DNS to assess combustion models for MILD combustion. The final section summarizes the key findings discussed in this chapter and outlines outstanding challenges that DNS can help resolve in the understanding and modeling of MILD combustion.

2 DNS of MILD combustion

To the author's knowledge, DNS of MILD combustion has been mainly conducted for three different configurations: (i) an autoigniting mixing layer with MILD combustion mixture [18], premixed internal exhaust gas recirculation (EGR) MILD combustion [19], and nonpremixed internal EGR MILD combustion [20]. The particularities of each DNS are presented next.

2.1 DNS of the autoigniting mixing layer

The autoigniting mixing layer configuration is shown in Fig. 1. This configuration focuses on MILD combustion applications originating from jets in hot and diluted coflow. In this configuration, there is a central jet fuel surrounded by a coflow of preheated air mixed with products of combustion to achieve MILD combustion conditions. This jet in hot coflow configuration has been widely studied experimentally [8, 9, 11]. To perform the DNS of such a configuration, the numerical domain was simplified to a time-evolving shear layer, as shown in Fig. 1A. There is a central fuel jet surrounded by a hot and diluted coflow, flowing in the opposite direction, creating a shear layer. Due to the high temperature of the coflow, ignition occurs, and the time evolution of this shear layer is studied to obtain insights into the physics of MILD combustion. The time evolution of the temperature field in the mid z-plane is shown in Fig. 1B where the ignition of the mixing layer can be observed. The exact turbulence condition and configuration of that DNS are summarized in Table 1. In this simulation, the fuel considered is a mix of 50% methane/50% hydrogen in volume, and the oxidizer has the same composition as in the experiments from Dally et al. [8] (3% of oxygen, 85% of nitrogen, 6.5% of water, and 5.5% of carbon dioxide). The chemical mechanism used was the DRM19 mechanism [21].

2.2 DNS with internal EGR

Another MILD combustion configuration that was studied using DNS is the configuration where MILD combustion is achieved with internal exhaust gas recirculation. This is, for example, the case in the experiments in the furnaces studied in Wünning et al. [2] where the products of combustion are recirculated within the combustion chamber and, therefore, mixed with the inflowing fuel and air. To perform the DNS of such a configuration, the simulation was actually split into two phases as detailed in Minamoto et al. [22] and Doan et al. [20]. This two-stage process is illustrated schematically in Fig. 2. The first stage mimics the mixing of fuel, air, and exhaust gases yielding an inhomogeneous mixture field, which subsequently undergoes combustion in the second stage. The left box titled "preprocessing" in Fig. 2 represents the first stage, while the second stage represents the actual MILD combustion DNS. In this first preprocessing stage, the initial progress variable and associated scalar and turbulence fields are generated to mimic a distribution of burnt and unburnt gases, and with mixture fraction distribution for the nonpremixed cases. Then, a mixing DNS is simulated without chemical reactions in a periodic domain for about one large eddy turnover time (shorter than the minimum ignition delay time) to ensure that the scalar and flow fields have interacted sufficiently before the combustion commences. This

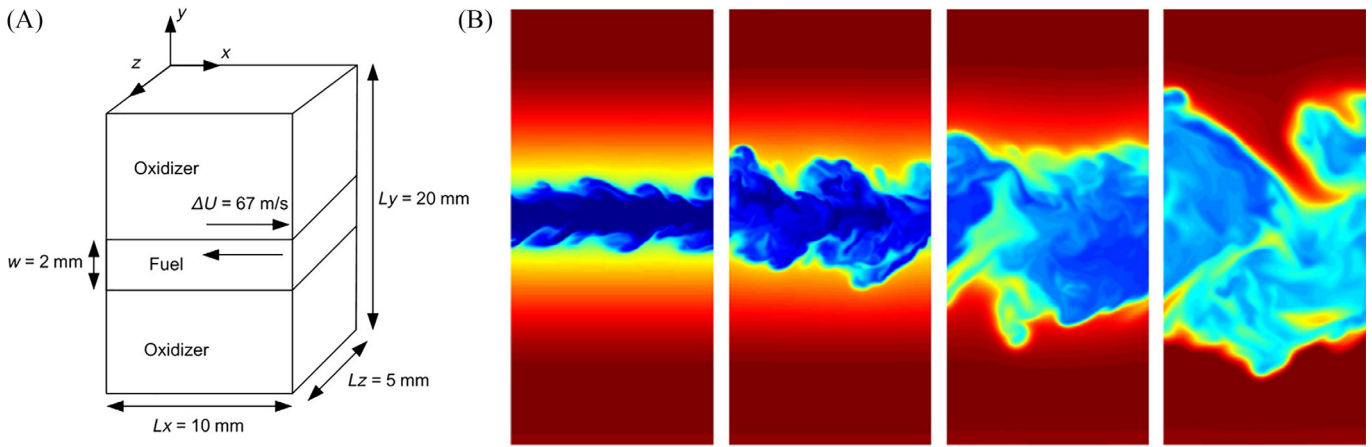

FIG. 1 (A) DNS configuration for the autoignition of a jet in hot coflow and (B) time evolution of the temperature field (range from 305 to 1285 K) in the mid z-plane. *Adapted from M.U. Göktolga, J.A. van Oijen, L.P.H. de Goey, 3D DNS of MILD combustion: a detailed analysis of heat loss effects, preferential diffusion, and flame formation mechanisms, Fuel 159 (2015) 784–795, https://doi.org/10.1016/j.fuel.2015.07.049.*

TABLE 1 DNS condition of the DNS of the autoigniting mixing layer from Göktolga et al. [18].

Parameter	
Fuel jet width	2 mm
Domain size ($L_x \times L_y \times L_z$)	10 mm × 10 mm × 5 mm
Grid points ($N_x \times N_y \times N_z$)	253 × 505 × 127
Relative velocity between fuel and oxidizer ΔU	67 m/s
Initial jet Reynolds number	3870
Initial turbulence fluctuations $u'/\Delta U$	0.05
Taylor microscale Reynolds number Re_λ	186
Turbulent kinetic energy k	55 $\mathrm{m}^2/\mathrm{s}^2$
Kolmogorov length scale η	0.024 mm

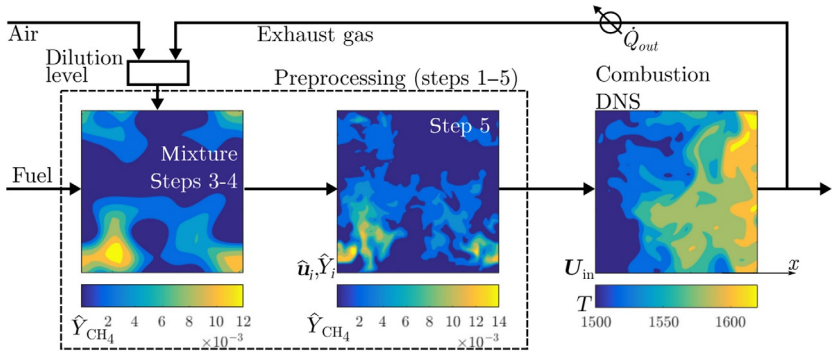

FIG. 2 Schematic illustration of the DNS steps for the simulation of MILD combustion with internal EGR. *Adapted from N.A.K. Doan, N. Swaminathan, Y. Minamoto, DNS of MILD combustion with mixture fraction variations, Combust. Flame 189 (2018) 173–189, https://doi.org/10.1016/j.combustflame.2017.10.030.*

reproduces the conditions obtained from EGR found in MILD combustion. In the second stage, this inhomogeneous mixture is used as the initial and inflowing mixture for the combustion simulation. Details of this procedure are provided in Minamoto et al. [22] and Doan et al. [20] for premixed and nonpremixed MILD combustion, respectively. The main difference between the preprocessing stage of those studies is that the work by Doan et al. [20] requires additional variations of the mixture fraction field, which reflects nonpremixed conditions.

The particular turbulence and thermochemical conditions of the premixed (cases A1, A2, B1, and C1) and nonpremixed MILD combustion (cases AZ1, AZ2, and BZ1) DNS from Minamoto et al. [22] and Doan et al. [20] are summarized in Tables 2–4. The fuel considered for those

TABLE 2 Initial conditions of the MILD combustion DNS with internal exhaust gas recirculation.

Case	P/NP	Mech	Λ_0/ℓ_Z	$\langle X_{O_2} \rangle$	$X_{O_2}^{max}$	ℓ_Z/ℓ_c	$\langle Z \rangle$	Z_{st}	σ_Z	$\langle c \rangle$	σ_c
AZ1	NP	MS-58	0.60	0.0270	0.035	1.30	0.008	0.010	0.0084	0.56	0.26
AZ2	NP	MS-58	0.79	0.0285	0.035	1.01	0.008	0.010	0.0105	0.56	0.28
BZ1	NP	MS-58	0.60	0.0160	0.020	1.30	0.0046	0.0058	0.0057	0.56	0.26
A1	P	S.&G.	–	0.0350	0.048	–	0.011	0.014	–	0.50	0.3
A2	P	S.&G.	–	0.0350	0.048	–	0.011	0.014	–	0.50	0.3
B1	P	S.&G.	–	0.0250	0.035	–	0.008	0.010	–	0.50	0.3
C1	P	S.&G.	–	0.0250	0.035	–	0.008	0.010	–	0.50	0.3

P and NP stand for premixed and nonpremixed conditions, respectively. X_{O_2} denotes the mole fraction of O_2, $\langle \cdot \rangle$ is the volume average, and σ is the standard deviation of the specified quantity. MS-58 refers to the modified Smooke mechanism [20] and S.&G. refers to the Smooke and Giovangigli mechanism [23]. Λ_0: integral length scale. ℓ_Z, ℓ_c: prescribed length scale of mixture fraction, Z, and progress variable, c.

TABLE 3 Oxidizer composition for the MILD mixture of the MILD combustion DNS with internal exhaust gas recirculation.

Cases	$X_{O_2,\,ox}$	$X_{H_2O,\,ox}$	$X_{CO_2,\,ox}$	$X_{N_2,\,ox}$
A1-2	0.049	0.123	0.062	0.765
AZ1-2, B1, C1	0.035	0.134	0.067	0.764
BZ1	0.020	0.146	0.073	0.761

TABLE 4 Turbulence and temperature conditions for the MILD combustion DNS with internal exhaust gas recirculation.

Cases	Λ_0	u'	Re_t (Re_λ)	T_r [K]
A2	1.63	10.12	67 (26)	1500
C1	2.52	4.10	55 (28.83)	1300
Other cases	1.42	16.67	96 (34.73)	1500

Λ_0: the integral length scale in mm; u': root-mean square of the velocity fluctuations in m/s; Re_t and Re_λ: turbulent and Taylor microscale Reynolds numbers, respectively.

cases is methane, and typical snapshots for those DNS are shown in Fig. 3. The numerical domain for all cases except case C1 is a cuboid of size $L_x \times L_y \times L_z = 10 \times 10 \times 10\ \mathrm{mm}^3$ with inflow and nonreflecting Navier-Stokes characteristics boundary conditions outflow [24] in the x-direction and periodic conditions in the transverse, y and z, directions. This domain is presented in Fig. 3 where isosurfaces of normalized heat release are shown. For case C1, the domain is $30 \times 20 \times 20\ \mathrm{mm}^3$. To ensure that all chemical and turbulence length scales are resolved, a uniform grid of 384^3 for case B1, 756×504^2 for case C1, and 512^3 for the other cases is used to discretize the numerical domain [20, 25].

For the premixed MILD combustion DNS in Minamoto et al. [22], different cases are considered to assess the effect of turbulence intensity (as shown in Table 4 with case A2 which has a turbulence lower level than the other cases), dilution levels (as shown in Table 3 with case B1 that has an oxygen level lower than the other cases), and reactant temperature (case C1 as detailed in Table 4) on the physics of MILD combustion. The combustion mechanism used is the Smooke mechanism [23].

The nonpremixed MILD combustion cases by Doan et al. [20] share similarities with the premixed cases of Minamoto et al. [22] but have the significant difference that they include mixture fraction variations allowing to study the effect of mixture fraction stratification (case AZ2 having the strong mixture fraction stratification) and the interaction between lean and rich mixtures. In addition, an even more diluted case (case BZ1)

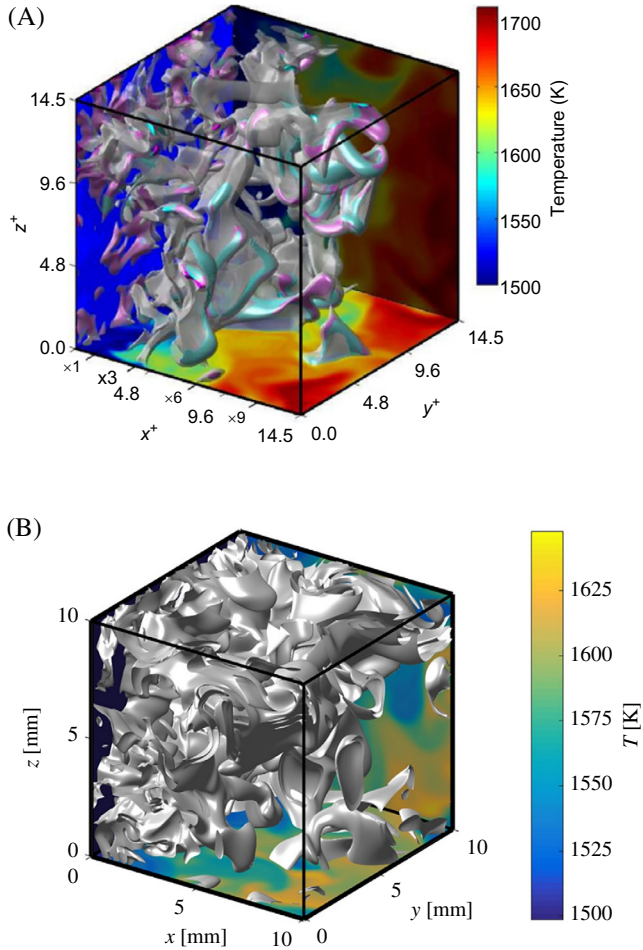

FIG. 3 Typical isosurface of normalized heat release rate for (A) case A1 and (B) case AZ1. Temperature field is shown on the bottom and side surfaces. *(A) Adapted from Y. Minamoto, T.-D. Dunstan, N. Swaminathan, R.S. Cant, DNS of EGR-type turbulent flame in MILD condition, Proc. Combust. Inst. 34 (2) (2013) 3231–3238, https://doi.org/10.1016/j.proci.2012.06.041; (B) Adapted from N.A.K. Doan, N. Swaminathan, Y. Minamoto, DNS of MILD combustion with mixture fraction variations, Combust. Flame 189 (2018) 173–189, https://doi.org/10.1016/j.combustflame.2017.10.030.*

has been performed by Doan et al. [20]. The combustion mechanism is a modified Smooke mechanism, as detailed in Doan et al. [20].

Typical isosurfaces of reaction rate for those simulations are shown in Fig. 3A for premixed MILD combustion and Fig. 3B for nonpremixed MILD combustion. In this figure, the complex nature of reaction zones in MILD combustion is evident. In contrast to conventional flames, which generally present a unique front, MILD combustion exhibits multiple

convoluted reaction zones, which can strongly interact with one another and, therefore, create an apparently distributed reaction zones [19, 20].

While it can be seen that the turbulent conditions of the DNS of MILD combustion mentioned earlier may seem quite different from the ones encountered in experiments, they nonetheless provide first insights into the physics of MILD combustion. In addition, the turbulence levels, and in particular the Reynolds number based on the integral length scale, indicated in Table 4 are of a similar order of magnitude as the ones carried out in experiments [25]. In addition, the Karlovitz number for these DNS is of $\mathcal{O}(10)$, which would put them in the thin reaction zones regime as defined in Peters [26]. However, this conventional regime diagram might not be as representative for MILD combustion as for conventional premixed combustion due to the presence of autoignition and the distributed nature of the reaction. Therefore, it may not be necessary to have very high turbulent flow for the generation of distributed reaction zones. Hence, a discussion using solely conventional Karlovitz or Damkohler numbers may be too limited to assess the MILD combustion conditions.

3 Physics of MILD combustion

The DNS described in Section 2 has enabled a finer understanding of the physics of MILD combustion. This section will summarize the findings of the studies by Göktolga et al. [18, 27], Minamoto et al. [22, 25, 28, 29], and Doan et al. [30–32]. In particular, findings regarding the inception of MILD combustion and the balance between ignition and deflagration will be discussed as well as their implications on the modeling framework necessary for MILD combustion.

3.1 Inception of MILD combustion: Jet in hot coflow configuration

In this section, the results obtained from the DNS of the autoigniting mixing layer introduced in Section 2.1 that analyzed the inception of MILD combustion are discussed. In particular, the results of Göktolga et al. [18] focused on the autoignition of a shear layer under MILD combustion conditions. In that case, it was observed that, due to the shear layer between the fuel jet and the hot oxidizer coflow, instabilities appeared, which grew into vortices. As the fuel spread wider into the hot oxidizer, ignition occurred, as illustrated in Fig. 1B. These ignition spots appeared at various locations along with this shear layer. Subsequently, the evolution of these ignition spots was analyzed using the species Damkohler number defined by Echekki and Chen [33]:

$$\mathrm{Da}_\alpha = \frac{\dot{\omega}_\alpha}{|\partial/\partial x_j(\rho Y_\alpha V_{j,\alpha})|} \tag{1}$$

where Y_α is the α-species mass fraction, $V_{j,\alpha}$ is the diffusive velocity in the jth direction and $\dot{\omega}_\alpha$ is the source term of species α. Da defined in such a way gives the relative importance between diffusive and chemical effects. Therefore, if Da is much larger than unity at regions not yet ignited, it means that those regions will undergo autoignition, given that chemical reactions dominate diffusion effects. Conversely, if Da is much smaller than unity in those regions, it means that the ignition of those regions will result from the diffusion of species into those regions from neighboring ignited ones depending on the diffusion direction. Therefore, those latter regions with Da < 1 would undergo a deflagration process. This analysis, based on hydrogen H, was performed by Göktolga et al. [18], and the results are shown in Fig. 4, where the numerator (chemical source term) and denominator (diffusion term) of Eq. (1) are shown.

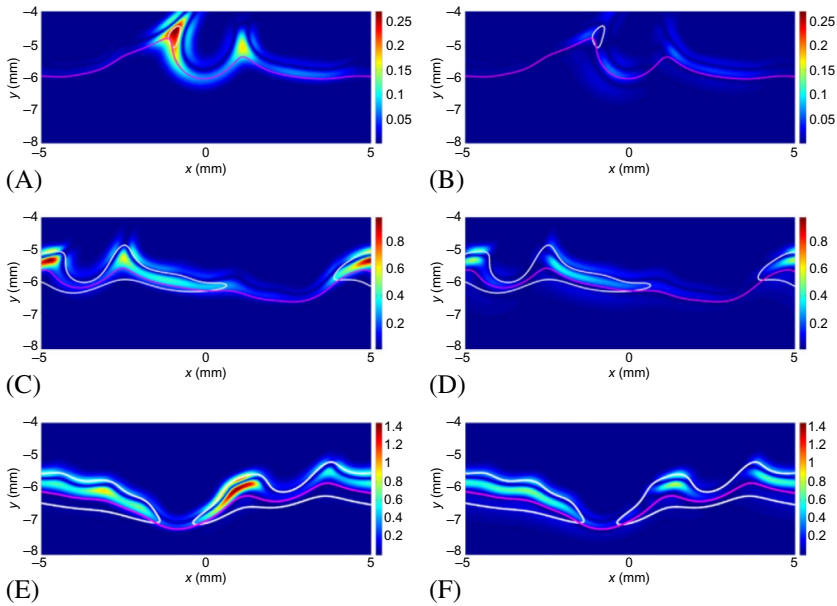

FIG. 4 Source and diffusion terms of H radical for the 3D case at $z = 0$ mm plane and at $t =$ 1.0, 1.1, and 1.2 ms. The *white contours* show the threshold value of $Y_H = 2 \times 10^{-5}$ and the *magenta lines* show $Z_{MR} = 2.5 \times 10^{-3}$. Z_{MR} is the most reactive mixture fraction, that is, the mixture fraction that has the lowest ignition delay time. Source term: (A) 1.0 ms, (C) 1.1 ms, (E) 1.2 ms; diffusion term: (B) 1.0 ms, (D) 1.1 ms, (F) 1.2 ms. (For interpretation of the references to colour in this figure legend, the reader is referred to the web version of this chapter.) *Adapted from M.U. Göktolga, J.A. van Oijen, L.P.H. de Goey, 3D DNS of MILD combustion: a detailed analysis of heat loss effects, preferential diffusion, and flame formation mechanisms, Fuel 159 (2015) 784–795, https://doi.org/10.1016/j.fuel.2015.07.049.*

In that figure, the evolution of the shear layer shortly after a first ignition is shown. It is seen that for the first time instant at $t = 1$ ms in the igniting region (regions enclosed by a white line, determined by regions where the H radical reached a given threshold), reaction effects dominate diffusion effects. More importantly, just outside of this reacting region, the reaction term is also large (and larger than diffusion effects) indicating that the pocket will undergo full autoignition. In addition, another reacting region that is not ignited yet can also be observed. Those first igniting regions were strongly correlated with the most reactive mixture fraction, Z_{MR}, that is, the mixture fraction that has the lowest autoignition delay time, which agrees with conventional autoignition studies [17]. At the next time instant, the igniting regions remained the ones where the chemical source term is larger than the diffusion term. This signified that the inception of MILD combustion occurs from general autoignition occurring at various regions rather than through the development of a deflagrative structure or from the diffusion of species along the most reactive mixture fraction isoline. This finding was further supported by the analysis of HO_2 radical concentrations, which are a precursor of autoignition [33–35]. At the time instant just before those shown in Fig. 4, a large production of HO_2 radical had already occurred in many different areas suggesting that those will all undergo autoignition, but with different time delays. This variation in ignition delay time was suggested to originate from variations in the local temperature and scalar dissipation rate experienced by the particular igniting pocket.

The analysis described earlier strongly distinguishes MILD combustion from other conventional flames, where ignition only occurs initially and the flame stabilizes through the development of a deflagrative structure. In contrast, the evidence obtained from DNS [18] suggests that MILD combustion occurs as a result of continuous autoignition with a strong influence of the mixture fraction and scalar dissipation rate on the sequence of ignition. Therefore, modeling attempts for MILD combustion will have to be able to accurately predict such evolution.

3.2 Inception of MILD combustion: Role of chemical radicals

In contrast to the DNS analysis discussed in the previous section by Göktolga et al. [18], analysis done in the DNS with internal EGR of nonpremixed MILD combustion by Doan and Swaminathan [31] highlighted the important role of chemical radicals in the inception and stabilization of MILD combustion, in addition to the mixture fraction. To do this, a quantity called the *incoming* radical concentration was studied. This incoming radical is defined as $\Delta Y_\alpha = Y_\alpha - Y_\alpha^c$, where Y_α^c is the local value of the *incoming* species where there is no combustion. This quantity was

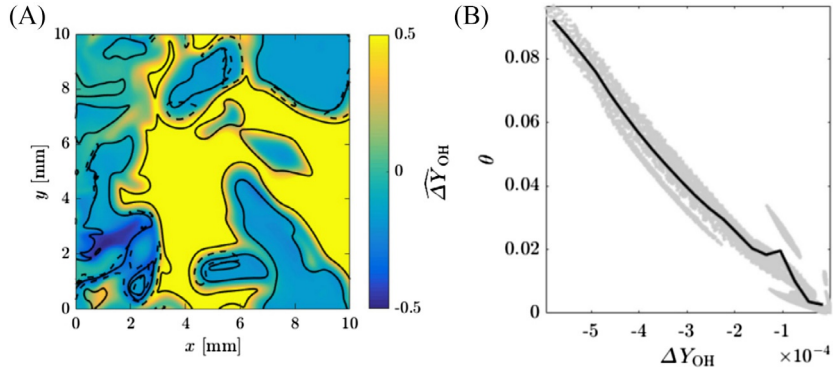

FIG. 5 (A) Variation of $\widehat{\Delta Y}_{OH} = \Delta Y_{OH}/\max(\Delta Y_{OH})$ in the mid x-y plane for case AZ1 and (B) variation of ΔY_{OH} with temperature increase $\theta = (T - T_r)/(T_p - T_r)$. *Adapted from N.A.K. Doan, N. Swaminathan, Role of radicals on MILD combustion inception, Proc. Combust. Inst. 37 (4) (2019) 4539–4546, https://doi.org/10.1016/j.proci.2018.07.038.*

obtained by performing a DNS with the same initial and inflowing fields as in the reacting DNS but where all chemical reactions are removed. As a result, the purely convective-diffusive evolution for the species inside the computational domain with the same turbulence field is obtained. Since the temperature rise in the MILD combustion DNS is moderate, the velocity fields in the reactive and nonreactive DNS are similar, especially in regions close to the inlet. A variation of ΔY_{OH} is shown in Fig. 5. This ΔY_{OH} quantity allows us to interpret whether a species concentration at a given location originates from convective-diffusive effects or whether it originates from chemical reactions, therefore allowing one to understand the local influence of combustion on these species. Therefore, $\Delta Y > 0$ indicates that OH is locally produced by combustion since the local Y_{OH} is larger than Y^c_{OH}. In Fig. 5, it is seen that OH is mostly negative in the upstream ($x \approx 0$) region. This indicates that the incoming OH is consumed by chemical reactions. Thus, the OH in the incoming recirculated exhaust gases is consumed and acts as a precursor for initiating ignition and heat release. The importance of radical consumption for the inception of MILD consumption was further highlighted by analyzing the correlation between temperature increase and ΔY_{OH}, shown here in Fig. 5B. In this figure, a robust correlation is observed between the ΔY_{OH} and the normalized temperature increase θ, which further supports that the inception of MILD combustion with internal EGR is driven by the consumption of recirculating radicals.

The discussion here shows that, in addition to the importance of the mixture fraction shown in the previous section [18], the recirculating radicals play a vital role in the inception of MILD combustion. This adds a new layer of complexity in the modeling of MILD combustion that,

therefore, must be able to account for radicals in their initial mixture and that the chemistry cannot be overly simplified.

3.3 Ignition and deflagration

As discussed in Section 1, the main interrogation in MILD combustion concerns the balance between ignition and deflagration. Experimental studies have shown competing views on this topic, and a more precise understanding is necessary for the appropriate modeling of MILD combustion. Indeed, many modeling frameworks, such as flamelet-generated manifold (FGM) or presumed PDF approaches, rely on some form of canonical flames. Therefore, understanding this balance between ignition and deflagration would enable a more judicious choice for such a modeling approach.

3.3.1 Combustion mode as balance in the transport equation

Investigations in this area were conducted by Minamoto et al. [25] and Doan and Swaminathan [30], where this balance between ignition and deflagration in MILD combustion with internal recirculation was studied in DNS of MILD combustion in premixed and nonpremixed internal recirculation configurations (described in Section 2.2). These analyses relied on computing the balance between the different terms in the species transport equation for some specific species. Indeed, this equation reads

$$\frac{\partial \rho Y_\alpha}{\partial t} + \underbrace{\frac{\partial \rho u_j Y_\alpha}{\partial x_j}}_{\mathcal{C}:\, conv.} = \underbrace{\frac{\partial}{\partial x_j}\left(\rho D_\alpha \frac{\partial Y_\alpha}{\partial x_j}\right)}_{\mathcal{D}:\, diff.} + \underbrace{\dot{\omega}_\alpha}_{\mathcal{R}:\, react.} \tag{2}$$

From this equation, turbulent combustion can be interpreted as a balance between convection, diffusion, and chemical reactions. As a result, the balance between these phenomena was analyzed using the following indicator:

$$\mathcal{B} \equiv |\mathcal{C} - \mathcal{D}| - |\mathcal{R}| \tag{3}$$

The previous equation suggests that regions with $\mathcal{B} < 0$ have a dominant reaction source can thus be taken to be similar to perfectly stirred reactors (PSR) and are thus ignition-dominated regions. Conversely, when $\mathcal{B} \approx 0$, there is a balance between convection, diffusion, and reaction, meaning that the regions with $\mathcal{B} \approx 0$ are similar to a steady flame and, therefore, the combustion mode in those regions is deflagrative. Typical contours of this $\mathcal{B}$ indicator are shown in Fig. 6 for reacting regions from Doan and Swaminathan [30] in the nonpremixed MILD combustion configuration, where H_2O was used as a species to compute $\mathcal{B}$. It can be seen that there is a coexistence of deflagrative and igniting regions. This was also

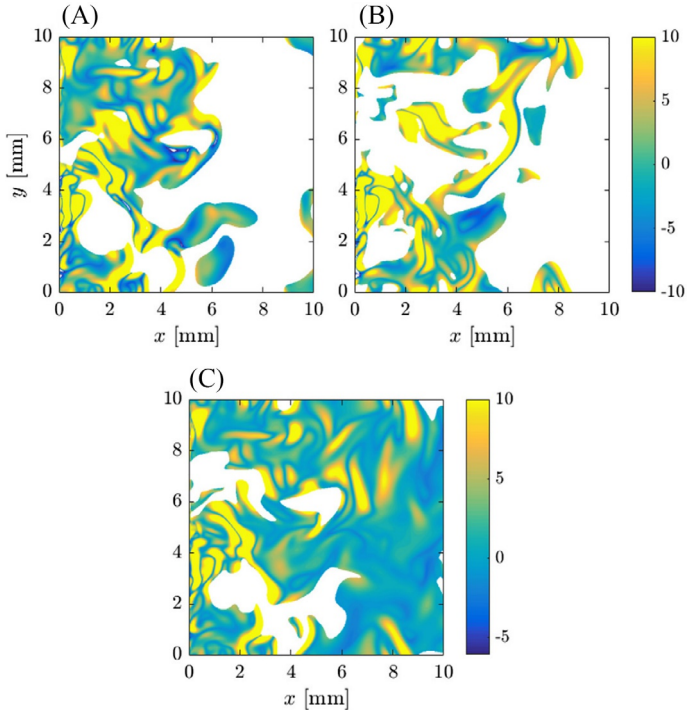

FIG. 6 Typical spatial variation of $\mathcal{B}$ in regions with normalized heat release rate, $\dot{Q}^{+} = \dot{Q}\delta_{th}/(\rho_r s_L C_p(T_p - T_r))$, larger than 1.0 at $t = 1.5\tau_f$ for cases (A) AZ1, (B) AZ2, and (C) BZ1. s_L is the laminar flame speed, C_p is the mixture heat capacity, δ_{th} is the laminar flame thermal thickness. *Adapted from N.A.K. Doan, N. Swaminathan, Autoignition and flame propagation in non-premixed MILD combustion, Combust. Flame 201 (2019) 234–243, https://doi.org/10.1016/j.combustflame.2018.12.025.*

observed in the DNS of premixed MILD combustion in Minamoto et al. [25], but where $\mathcal{B}$ is based on the temperature progress variable c_T.

In premixed MILD combustion with internal EGR, a finer analysis showed that in the upstream stage of the domain, ignition ($\mathcal{B} < 0$) was the most probable combustion mode (see Fig. 7). However, as one moves downstream, the most probable combustion mode shifts from ignition toward deflagration ($\mathcal{B} \approx 0$). However, in nonpremixed MILD combustion, Doan, and Swaminathan [30] highlighted a different behavior. More specifically, there was a strong dependence of the combustion mode on the mixture fraction stratification. In particular, conditions that exhibited low mixture stratification showed similar behavior as the premixed MILD combustion cases of Minamoto et al. [25] shown in Fig. 7, namely a transition from ignition toward deflagration as one moves downstream in the domain (see Fig. 8A where the peak of the PDF of $\mathcal{B}$close to zero increases).

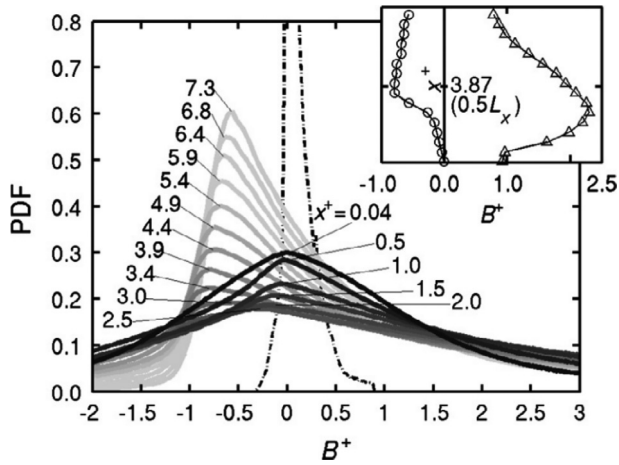

FIG. 7 PDF of $\mathcal{B}$ at various axial $x^+ = x/\delta_{th}$ positions in Case B1. The PDF is also shown for a typical premixed combustion case (*dash-dotted line*). The *inset* shows the variation of the most probable (*circles*) and averaged (*triangles*) values of $\mathcal{B}$ along x^+. *Adapted from Y. Minamoto, N. Swaminathan, R.S. Cant, T. Leung, Morphological and statistical features of reaction zones in MILD and premixed combustion, Combust. Flame 161 (11) (2014) 2801–2814, https://doi.org/10.1016/j.combustflame.2014.04.018.*

However, when strong mixture stratification was present, and hence the level of premixing was small, the autoignition mode remained throughout the computational domain as shown in Fig. 8B, where the $\mathcal{B}$ analysis was performed on the case AZ2 (discussed in Section 2.2) that has strong mixture fraction stratification. This is in contrast with premixed MILD combustion but indicates similar findings to the autoignition shear layer studied by Göktolga et al. [18]. A finer analysis of that particular DNS condition highlighted that sequential autoignition was occurring: ignition first occurred in the lean mixture, close to the most reactive mixture fraction, and the richer mixture only ignited subsequently. This was supported by analyzing the evolution of the fuel pocket: a rich fuel mixture (richer than the rich flammability limit) first had to mix with the oxidizer before undergoing ignition. Therefore, this DNS by Doan and Swaminathan [30] shares similarities with the findings of Göktolga et al. [18] discussed previously but emphasizes the effect of mixture fraction (and its mixing) on the ignition delay time rather than temperature and scalar dissipation rate of mixture fraction that results in this sequential autoignition behavior.

This influence of the mixture fraction on the combustion mode was further analyzed in a statistical sense. Using the $\mathcal{B}$-indicator, it was observed that, as one moves downstream, first lean then close to the stoichiometric mixture are undergoing autoignition as shown in Fig. 9, further

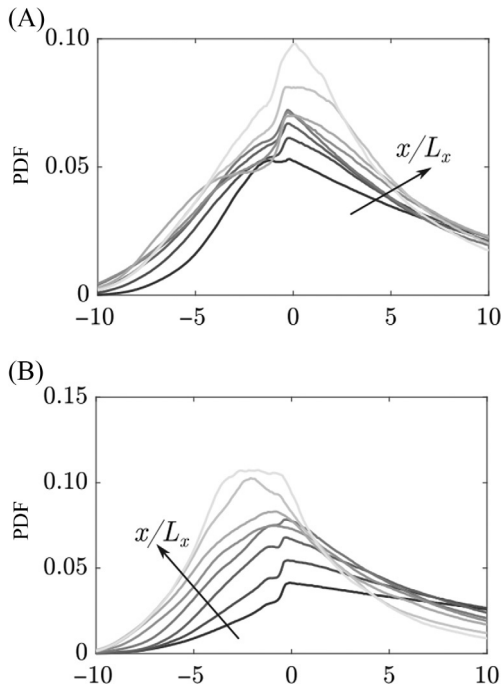

FIG. 8 PDF of $(\mathcal{B}|\dot{Q}^+ > 1.0)$ at $x/L_x = 0.0625, 0.1875, 0.3125, \ldots, 0.9375$ (*dark to light gray*) for cases (A) AZ1 and (B) AZ2. *Adapted from N.A.K. Doan, N. Swaminathan, Autoignition and flame propagation in non-premixed MILD combustion, Combust. Flame 201 (2019) 234–243, https://doi.org/10.1016/j.combustflame.2018.12.025.*

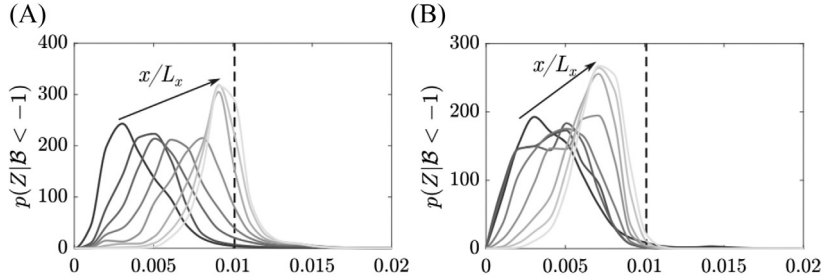

FIG. 9 PDF of $(Z|\mathcal{B} < -1.0)$ at $x/L_x = 0.0625, 0.1875, 0.3125, \ldots, 0.9375$ (*dark to light gray*) for cases (A) AZ1 and (B) AZ2. The *dashed lines* indicate the stoichiometric mixture fraction. *Adapted from N.A.K. Doan, N. Swaminathan, Autoignition and flame propagation in non-premixed MILD combustion, Combust. Flame 201 (2019) 234–243, https://doi.org/10.1016/j.combustflame.2018.12.025.*

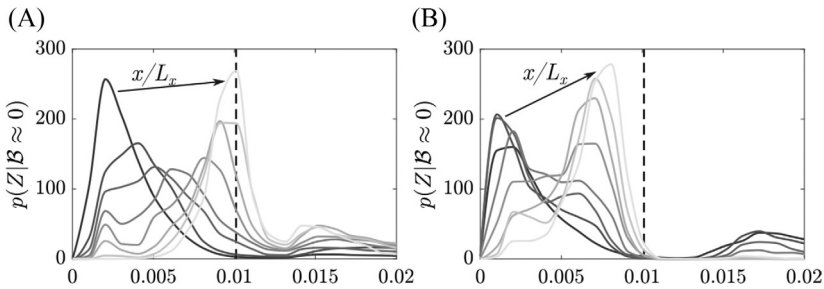

FIG. 10 PDF of $(Z| - 0.1 \leq \mathcal{B} \geq 0.1)$ at $x/L_x = 0.0625, 0.1875, 0.3125, \ldots, 0.9375$ (*dark to light gray*) for cases (A) AZ1 and (B) AZ2. The *dashed lines* indicate the stoichiometric mixture fraction. *Adapted from N.A.K. Doan, N. Swaminathan, Autoignition and flame propagation in non-premixed MILD combustion, Combust. Flame 201 (2019) 234–243, https://doi.org/10.1016/j.combustflame.2018.12.025.*

supporting this sequential autoignition. However, when focusing on the mixture fraction in deflagrative mode ($\mathcal{B} \approx 0$), one observed differences again depending on the mixture fraction stratification, as shown in Fig. 10. In the case of small mixture fraction stratification (Fig. 10A), both the presence of lean and rich flame-like structures can be observed. In the early stage of the domain, only lean deflagrative structures are observed. As one moves downstream, the typical mixture fraction in those deflagrative structures increases, and stoichiometric and rich flame-like structures can be observed. Those rich flames, however, do not originate from a rich mixture that ignited, but rather, they come from the propagation of an initially lean or stoichiometric flame that propagates into a richer mixture. Indeed, no rich igniting kernels were observed in the DNS of Doan and Swaminathan [30]. In contrast, when strong mixture stratification is present (Fig. 10B), rich flame-like structures can already be observed in the upstream region. This originates from the smaller mixture fraction length scale that indicates that rich mixtures may be closer to leaner ones. Therefore, a deflagative structure that is originally lean will quickly encounter a richer mixture.

3.3.2 Combustion mode from chemical explosive mode analysis

A final approach to analyze this balance between ignition and deflagration in MILD combustion was studied in Doan et al. [32], where the chemical explosive mode analysis (CEMA) methodology was used on the DNS datasets of Minamoto et al. and Doan et al. presented in Section 2.2. This approach, initially developed by Lu et al. [36], is based on the analysis of the eigenvalues, λ_e, of the Jacobian of the local chemical source term, $\boldsymbol{J}_{\boldsymbol{\omega}}$. The original CEMA method has been extended to account for diffusion effects to distinguish between combustion modes [37, 38]. This is obtained from

$$\frac{D\dot{\boldsymbol{\omega}}(\boldsymbol{y})}{Dt} = \boldsymbol{J}_{\boldsymbol{\omega}} \frac{D\boldsymbol{y}}{Dt} = \boldsymbol{J}_{\boldsymbol{\omega}}(\dot{\boldsymbol{\omega}} + \boldsymbol{s}), \quad \boldsymbol{J}_{\boldsymbol{\omega}} = \frac{\partial \dot{\boldsymbol{\omega}}}{\partial \boldsymbol{y}} \tag{4}$$

where $\boldsymbol{y}$ represents the species concentrations and temperature, $\dot{\boldsymbol{\omega}}$ is the chemical source term, and $\boldsymbol{s}$ is the nonchemical term representing effects such as diffusion or homogeneous mixing. A chemical explosive mode (CEM) exists if one of the eigenvalues of the Jacobian, λ_e, has a positive real part. To distinguish between the different combustion modes, Eq. (4) is projected in the direction of the corresponding left eigenvectors, $\boldsymbol{b}_e$, of $\boldsymbol{J}_{\boldsymbol{\omega}}$:

$$\boldsymbol{b}_e \cdot \frac{D\dot{\boldsymbol{\omega}}(\boldsymbol{y})}{Dt} = \boldsymbol{b}_e \cdot \boldsymbol{J}_{\boldsymbol{\omega}}(\dot{\boldsymbol{\omega}} + \boldsymbol{s}) = \lambda_e \boldsymbol{b}_e \cdot (\dot{\boldsymbol{\omega}} + \boldsymbol{s}) \tag{5}$$

Then, the expression for the projected source term is

$$\frac{D\phi_{\omega}}{Dt} = \lambda_e \phi_{\omega} + \lambda_e \phi_s + \frac{D\boldsymbol{b}_e}{Dt} \cdot \dot{\boldsymbol{\omega}}(\boldsymbol{y}) \tag{6}$$

where $\phi_{\omega} = \boldsymbol{b}_e \cdot \dot{\boldsymbol{\omega}}$ and $\phi_s = \boldsymbol{b}_e \cdot \boldsymbol{s}$ are, respectively, the projected chemical and diffusion terms. The ratio $\alpha = \phi_s/\phi_{\omega}$ can then be used to indicate the relative importance of diffusion and chemistry. Based on the values of α, three regimes can be identified: $\alpha > 1$ for assisted-ignition mode where diffusion dominates chemistry and promotes ignition, $|\alpha| < 1$ for autoignition where chemistry is predominant, and $\alpha < -1$ for the local extinction mode, where diffusion suppresses ignition. Details on this method can be found in various studies [37–39], where it has already been applied successfully. Those findings suggested that CEMA was an appropriate candidate to analyze the balance between ignition and deflagration in MILD combustion.

One of the main advantages of CEMA compared to the use of the $\mathcal{B}$ criterion proposed in Doan and Swaminathan [30] and discussed in the previous section, is that it does not require to decide on a specific species for the analysis. Indeed, the $\mathcal{B}$ indicator can provide conflicting indications depending on the species used to define $\mathcal{B}$. In contrast, CEMA provides a unique indicator through the eigenvalue, λ_e, which has the most significant positive real part.

This analysis of the combustion modes in MILD combustion based on CEMA was performed by Doan et al. [32]. Fig. 11 shows the α indicator based on CEMA for some typical DNS of MILD combustion with internal EGR. The figures highlight that most cases exhibit large autoignition regions ($\alpha \approx 0$) with patches of deflagrative structures ($\alpha \geq 1$). However, the premixed case B1, in Fig. 11C, shows that the deflagrative mode is more likely in the upstream region of the domain when compared with the nonpremixed cases. The more specific balance between those modes was further studied statistically, where the probability density function (PDF) of this α indicator was computed (shown in Fig. 12). It is seen that,

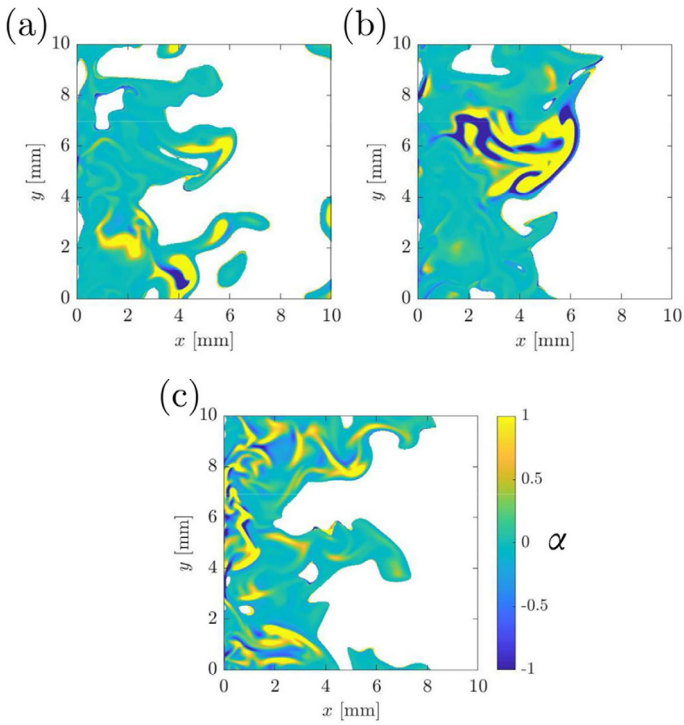

FIG. 11 Typical distribution of α in regions with $\lambda_e > 0$ in the mid x-y plane for cases (A) AZ1, (B) AZ2, and (C) B1. *Adapted from N.A.K. Doan, S. Bansude, K. Osawa, Y. Minamoto, T. Lu, J.H. Chen, N. Swaminathan, Identification of combustion mode under MILD conditions using chemical explosive mode analysis, Proc. Combust. Inst. (2021), https://doi.org/10.1016/j.proci.2020.06.293.*

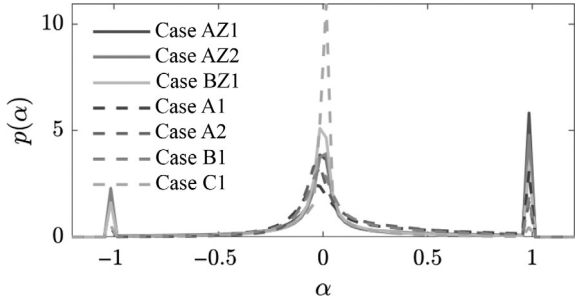

FIG. 12 PDF of α in regions with $\lambda_e > 0$ for all the DNS cases from Doan et al. [32]. *Adapted from N.A.K. Doan, S. Bansude, K. Osawa, Y. Minamoto, T. Lu, J.H. Chen, N. Swaminathan, Identification of combustion mode under MILD conditions using chemical explosive mode analysis, Proc. Combust. Inst. (2021), https://doi.org/10.1016/j.proci.2020.06.293.*

overall, cases AZ1 and AZ2 show that $\alpha \geq 1$, and thus flame propagation is the most likely mode but that both ignition and deflagration are nearly balanced. Case BZ1 and all the other premixed cases show that $\alpha = 0$, and thus ignition, is the most critical combustion mode.

However, a finer analysis of the combustion mode depending on the axial locations showed a different picture. In this case, the PDF of α conditioned of the axial location, shown in Fig. 13, was analyzed to understand the evolution of the combustion mode. This analysis showed a strong dependency of the combustion mode for nonpremixed MILD combustion, where cases with strong mixture stratification (low level of fuel/oxidizer premixing) showed a sequential autoignition mode (see Fig. 13B), similar to the physics of SCCI systems with mixture fraction stratification [40] or in HCCI systems with temperature stratification [41]. The stronger mixture fraction stratification hinders the development of flame fronts. Furthermore, because of this stronger mixture stratification, the various pockets of mixtures undergo ignition independently depending on their mixture fraction and local conditions [30]. In contrast, when there is a low mixture fraction stratification, as one traverses downstream, ignition (the peak of $p(\alpha) = 0$) becomes less important while flame propagation

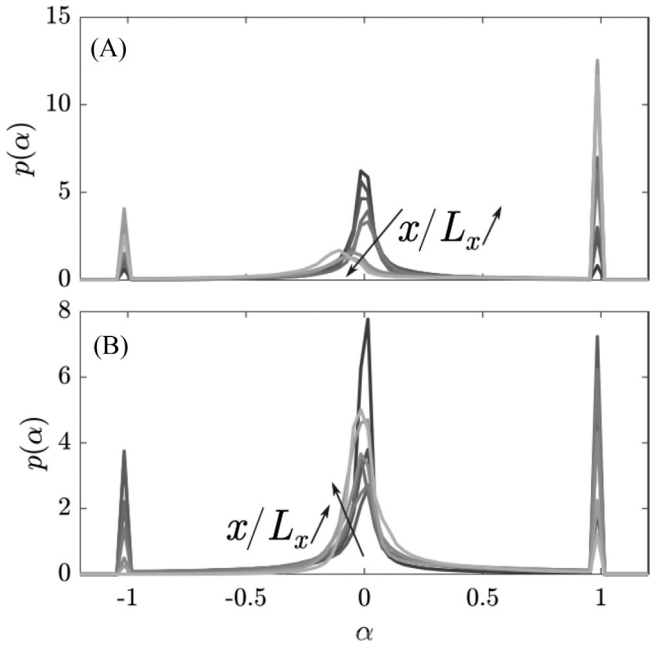

FIG. 13 Evolution of $p(\alpha)$ at various axial locations: $x/L_x = 0.03125, 0.15625, \ldots, 0.90625$ (from upstream to downstream: *black to light gray*) for cases (A) AZ1 and (B) AZ2 at $t = 1.5\tau_f$. *Adapted from N.A.K. Doan, S. Bansude, K. Osawa, Y. Minamoto, T. Lu, J.H. Chen, N. Swaminathan, Identification of combustion mode under MILD conditions using chemical explosive mode analysis, Proc. Combust. Inst. (2021), https://doi.org/10.1016/j.proci.2020.06.293.*

TABLE 5 Fractional contribution of the combustion modes to the total heat release rate in the domain for all MILD combustion cases.

Case	$\mathcal{Q}_{fl}$	$\mathcal{Q}_{ign}$	$\mathcal{Q}_{ext}$
AZ1	0.0753	0.8877	0.0370
AZ2	0.0551	0.9111	0.0338
BZ1	0.0503	0.9258	0.0239
A1	0.0436	0.9430	0.0134
A2	0.0274	0.9593	0.0052
B1	0.0311	0.9673	0.0096
C1	0.0067	0.9869	0.0064

becomes dominant (see Fig. 13A). This indicates that ignition kernels evolve into propagating flames in this case. This particular behavior was also observed for all the DNS of premixed MILD combustion. In addition, the mixture fraction of those ignition or deflagration structures was further analyzed. The analysis showed that ignition ($|\alpha| < 1$) is mostly present in lean mixtures, which are consistent with conventional autoignition, where lean mixtures are more likely to ignite [17]. On the other hand, deflagrative structures ($\alpha > 1$) are mostly present in rich mixtures.

Despite the coexistence of ignition and deflagration structures, the overall contributions of those different combustion modes to the total heat release rate highlighted a striking result, as shown in Table 5 where the fractional contribution of each combustion mode to the total heat release rate is shown. Despite the large probability of finding a deflagrative mode, those regions only contributed to a very small portion of the total heat release rate in the computational domain, where over 85% of the total heat release rate is due to autoignition. This indicated that while there may be a volumetric distribution of a deflagrative mode, MILD combustion is mostly controlled by ignition processes.

3.3.3 *Summary*

The various works discussed in this section [25, 30, 32] illustrated the coexistence and intertwined nature of ignition and deflagration in MILD combustion. While they may interact strongly spatially, the key observation from all those studies were that autoignition was the main driver of heat release rate in MILD combustion. This has large consequences for the modeling of MILD combustion as it suggests that modeling based on deflagrative flames (such as flamelets approaches) may not be appropriate. Such discussions on the modeling of MILD combustion will be presented in the following section.

4 Modeling insights: A priori analysis from DNS

In this section, the modeling insights obtained from DNS will be discussed. Indeed, from DNS data, modeling frameworks can be tested in an a priori setting, meaning that the DNS data are filtered to deduce RANS or LES-like quantities from which the modeled quantities, such as the modeled reaction rates, are computed and compared to the actual filtered quantity. This is key in correctly developing a modeling framework for MILD combustion. The various modeling strategies tested a priori are presented in the following few sections.

4.1 Presumed PDF approach

In many studies [18, 28, 29, 42], a flamelet-like model with presumed PDF is used as a modeling framework for the reaction rate of MILD combustion. In this framework, the filtered reaction rate is related to a canonical 0 or 1D laminar flame, such as a laminar premixed flame or a perfectly stirred reactor (PSR) through:

$$\widetilde{\dot{\omega}_\alpha} = \overline{\rho} \int_0^1 \dot{\omega}_\alpha^L(\eta) p(\eta) d\eta \tag{7}$$

where $\dot{\omega}_\alpha^L$ is the reaction rate of species α in a canonical laminar configuration, p is the modeling or subgrid PDF (often a β-PDF approach is used), and η is the sampling variable. The $\widetilde{\cdot}$ indicates the Favre-filtered quantity and $\overline{\cdot}$ indicates the average quantity. It is evident that for this modeling framework to be accurate, an appropriate choice of canonical configuration from which to compute $\dot{\omega}_\alpha^L$ must be made and that an accurate PDF p must be chosen. This choice of this canonical configuration has been studied in work mentioned earlier, and their results are discussed here.

Minamoto and Swaminathan [28] compared the use of flamelets and PSR in a RANS context and analyzed the accuracy of the model. This choice of either flamelet or PSR for this canonical configuration was based on the observations reported in Section 3.3, where both deflagrative and autoignition structures were observed. The flamelet was based on the 1D laminar premixed flame that had the same composition as the volume average mixture (where radicals and intermediates are excluded) in the inflowing MILD combustion DNS, while the PSR was based on the volume average mixture of the inflowing MILD combustion (including radicals and intermediates). This decision to use the volume average mixture was necessary to account for the presence of exhaust gas pockets in the inflowing MILD combustion mixture. It was observed that the PSR approach provided a better agreement with the averaged reaction rate from DNS compared to the flamelet. This is in line with the results

reported in Section 3.3, where various studies showed that ignition was the dominant mode of combustion in MILD combustion.

This modeling framework proposed in a RANS context was further assessed in an LES context in related work [29]. In this case, the averaging operation in RANS is replaced by a filtering operation:

$$\overline{f}(\boldsymbol{x}) = \int_{\Delta} f(\boldsymbol{x}')G(\boldsymbol{x}-\boldsymbol{x}';\Delta)d\boldsymbol{x}' \tag{8}$$

where $\boldsymbol{x}$ is the spatial coordinate and G is the Gaussian kernel with filter size Δ given by

$$G(\boldsymbol{x}-\boldsymbol{x}';\Delta) = \left(\frac{6}{\pi\Delta^2}\right)^{1/2} \exp\left(\frac{-6(\boldsymbol{x}-\boldsymbol{x}')^2}{\Delta^2}\right) \tag{9}$$

Similar to the analysis in a RANS context performed in Minamoto and Swaminathan [28], a comparison between PSR and flamelet configurations with the flame structures in the DNS highlighted that only the PSR could accurately capture the appropriate species and reaction rate evolution, as highlighted in Fig. 14. In this figure, it can be seen that the conditional average from the DNS is more accurately reproduced by the PSR than the flamelet (noted MIFE in the figure) configuration. In particular, the nonzero reaction rate at the inlet $x = 0$ location cannot be

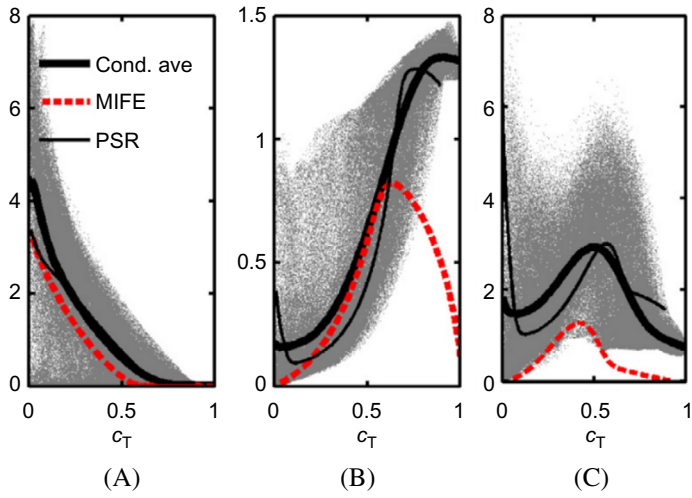

FIG. 14 Variations of (A) $Y_{CH_4}(\times 10^3)$, (B) $Y_{OH}(\times 10^3)$, and (C) $\dot{\omega}^+_{c_T} = \dot{Q}/(\rho C_p(T_p - T_r))$ with c_T. The scattered data are the DNS result at single time instant, *thick solid line* is the conditional averages, $\langle Y_\alpha|c_T\rangle$ (A and B) and $\langle\dot{\omega}^+_{c_T}|c_T\rangle$ (C), obtained from the DNS data collected over the entire sampling period, *red dashed line* is the flamelet (MIFE) solution, and *thin solid line* is the PSR result. *Adapted from Y. Minamoto, N. Swaminathan, Subgrid scale modelling for MILD combustion, Proc. Combust. Inst. 35 (3) (2015) 3529–3536, https://doi.org/10.1016/j.proci.2014.07.025.*

captured by the flamelet structure as the initial mixture does not contain radicals. However, the presence of radicals at the inception of MILD combustion was crucial, as discussed in Section 3.2 and in Doan and Swaminathan [31].

As a result, only the PSR-based model was assessed in the a priori setting. The filtered reaction rate and the modeled one are shown in Fig. 15. The modeled reaction rate can reproduce the filtered reaction rate field reasonably well for the different filter sizes considered. More quantitatively, an assessment of the accuracy of this PSR-based modeled reaction rate was performed by computing the joint PDF between the model and the filtered reaction rates and is shown in Fig. 16 for different filter sizes.

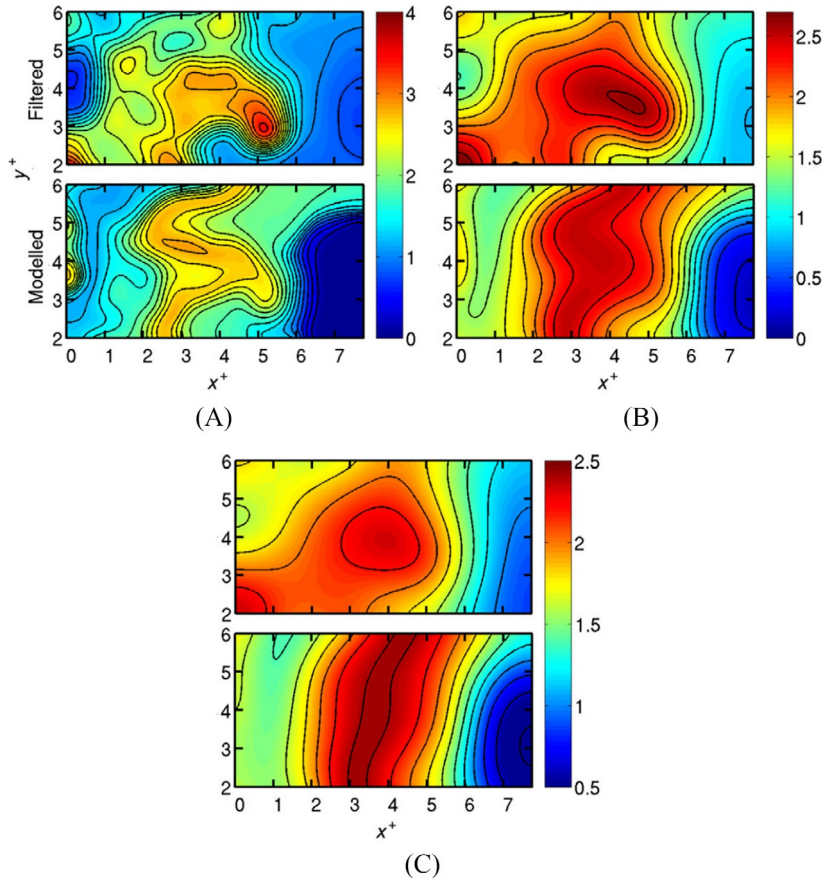

FIG. 15 Comparison of (*top*) $\overline{\dot{\omega}}^+_{c_T}$, (*bottom*) $\overline{\dot{\omega}}^+_{c_T,model}$ in the middle *x*-*y* plane at an arbitrary time instant for (A) $\Delta = \delta_{th}$, (B) $2\Delta = \delta_{th}$, and (C) $\Delta = 3\delta_{th}$. *Adapted from Y. Minamoto, N. Swaminathan, Subgrid scale modeling for MILD combustion, Proc. Combust. Inst. 35 (3) (2015) 3529–3536, https://doi.org/10.1016/j.proci.2014.07.025.*

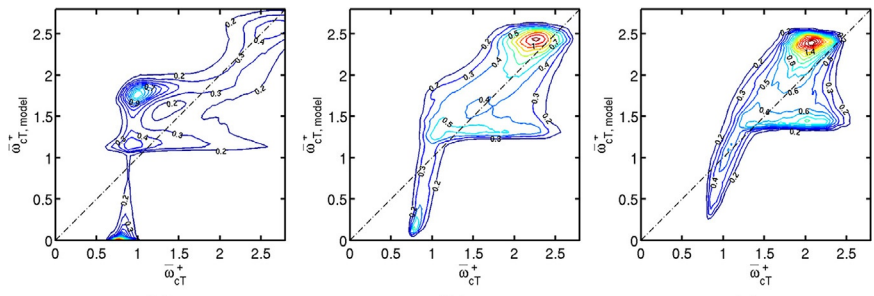

FIG. 16 The joint PDF of $\overline{\dot{\omega}}^{+}_{c_T}$ and $\overline{\dot{\omega}}^{+}_{c_T,model}$ computed using the DNS data from the entire sampling period for (A) $\Delta = \delta_{th}$, (B) $\Delta = \delta_{th}$, and (C) $\Delta = 3\delta_{th}$. *Adapted from Y. Minamoto, N. Swaminathan, Subgrid scale modeling for MILD combustion, Proc. Combust. Inst. 35 (3) (2015) 3529–3536, https://doi.org/10.1016/j.proci.2014.07.025.*

In this plot, a perfect agreement would translate into a spread around the diagonal line. As one can see, the model is more accurate for larger filter sizes, while for the smallest filter size ($\Delta^+ = 1$) some strong discrepancy can be observed. This is because the DNS of MILD combustion includes both autoigniting regions and deflagrative thin reaction zones, as discussed in Section 3.3. With large filter sizes, those thin regions are filtered out, but for small filter sizes, those thin reaction zones persist. However, these regions cannot be appropriately modeled by the PSR, and a flamelet-like model would be more appropriate. Another potential source of discrepancy could originate from the use of a β-PDF in Eq. (7).

This assessment of the appropriate PDF to use in Eq. (7) in the modeling of MILD combustion was further analyzed in Chen et al. [42] using the DNS with mixture fraction stratification of Doan et al. [20]. Compared to the previous a priori analyses [28, 29], which analyzed premixed MILD combustion, an additional complication stemmed from the need to model the joint progress variable/mixture fraction PDF. Indeed, in nonpremixed combustion, the equation for the modeled reaction rate becomes

$$\widetilde{\dot{\omega}_c}(\boldsymbol{x},t) = \overline{\rho}(\boldsymbol{x},t)\int_0^1\int_0^1 \dot{\omega}^L(Z,c)\widetilde{p}(Z,c;\boldsymbol{x},t)dZdc \tag{10}$$

where $\widetilde{\cdot}$ indicates the Favre filtering, c is a reaction progress variable, Z is the mixture fraction, and $\dot{\omega}^L$ is the reaction rate from a canonical laminar configuration. In work by Chen et al. [42], the analysis is focused on assessing appropriate modeling for the subgrid PDF $\widetilde{p}$ and $\dot{\omega}^L(Z,c)$ is directly taken from the DNS data as the doubly conditioned mean reaction rate:

$$\dot{\omega}^L(Z,c) = \left\langle \frac{\dot{\omega}^{DNS}(\boldsymbol{x},t)}{\rho(\boldsymbol{x},t)}\middle| Z,c \right\rangle \tag{11}$$

This approach allows focusing solely on the discrepancies that originate from an approximate subgrid PDF. In that work, different modeling approaches were assessed. First, the use of β-PDF to model the PDF of Z and the PDF of c was considered, where the β-PDF is defined as

$$\widetilde{p}_\beta(\xi;\widetilde{Z},\widetilde{\sigma_Z^2}) = \frac{\Gamma(a+b)}{\Gamma(a)\Gamma(b)}\xi^{a-1}(1-\xi)^{b-1} \tag{12}$$

with $a = \widetilde{Z}(1/\widetilde{g_Z} - 1)$ and $b = (1-\widetilde{Z})(1/\widetilde{g_Z} - 1)$, Γ is the gamma function and $\widetilde{g_Z} = \widetilde{\sigma_Z^2}/(\widetilde{Z}(1-\widetilde{Z}))$ is the segregation factor. Using this β-PDF, two cases were considered. Either the PDF of progress variable and reaction rate were considered independent, leading to

$$\widetilde{p}(\xi,\eta) = \widetilde{p}_\beta(\xi;\widetilde{Z},\widetilde{\sigma_Z^2})\widetilde{p}_\beta(\eta;\widetilde{c},\widetilde{\sigma_c^2}) \tag{13}$$

Or, these PDFs were correlated, and the *copula* method was used to account for the cross-correlation between progress variable and mixture fraction. This latter approach was proposed by Darbyshire and Swaminathan [43] based on the Plakkett copula method [44]. In this case, the additional subgrid covariance $\widetilde{\sigma_{Z,c}}$ also has to be accounted for, and the associated joint PDF is computed as

$$\widetilde{p}(Z,c) = \frac{\theta\widetilde{p}_\beta(Z)\widetilde{p}_\beta(c)(\mathcal{A}-2\mathcal{B})}{(\mathcal{A}^2-4\theta\mathcal{B})^{3/2}} \tag{14}$$

where $\mathcal{A} = 1 + (\theta-1)[\widetilde{\mathcal{C}}_\beta(Z)+\widetilde{\mathcal{C}}(c)]$ and $\mathcal{B} = (\theta-1)\widetilde{\mathcal{C}}_\beta(Z)\widetilde{\mathcal{C}}_\beta(c)$ with $\widetilde{\mathcal{C}}$ being the β cumulative distribution function (cdf) and θ the odd ratio calculated using a Monte Carlo approach (see Darbyshire and Swaminathan [43] for more details on the copula approach). Finally, the last approach considered was to use a deep feedforward neural network (DNN) to model the subgrid PDF from filtered quantities ($\widetilde{Z}$, $\widetilde{\sigma_Z^2}$, $\widetilde{c}$, $\widetilde{\sigma_c^2}$, and $\widetilde{\sigma_{Z,c}}$). In this case, a four-layer feedforward neural network with LeakyReLU and batch normalization was used.

A typical joint PDF extracted from DNS data of case AZ1 is shown in Fig. 17, where the particular shape of the joint PDF is shown. The MILD combustion case AZ1 with small mixture fraction stratification exhibits a nearly bimodal joint PDF with a negative correlation between mixture fraction and progress variable. This aligned with the findings in Doan et al. [32,] which showed that case AZ1 had nonnegligible deflagrative-like structures, where this assumption of bimodality may be valid. In contrast, case AZ2, shown in Fig. 18, shows a quite different joint PDF where the PDF of the progress variable shows a peak but also a wide plateau which cannot be easily modeled using the β-PDF.

The modeling attempts of this joint PDF are shown in Fig. 19, where independent β-PDFs, correlated β-PDF with the copula method, and the

joint PDF obtained using DNN are compared when trying to model the joint PDF for an arbitrary point in case AZ2. It is evident that the approach based on DNN, proposed by Chen et al. [42], is the only approach that can reproduce with some level of accuracy the actual joint PDF. This was further confirmed quantitatively using the Jansen-Shannon divergence (JSD), which quantifies the discrepancy between probability density functions. This is shown in Fig. 20, where the PDF of JSD shows a peak much closer to zero (indicating a perfect match) for the DNN compared to the other modeling approaches.

The next step in assessing the joint PDF modeling was to analyze the modeled reaction rate using Eq. (10). A typical modeled reaction rate obtained so is shown in Fig. 21, where all models seem to qualitatively well reproduce the filtered reaction rate obtained from DNS. In that figure, $\overline{\dot{\omega}}_{c_T}^{m-DNS}$ indicates the best modeled reaction rate one can obtain when using a presumed PDF approach, as defined by Eq. (10), that is, where Eq. (10) is computed using all quantities coming from the DNS. That quantity is therefore used as a basis for comparison in Fig. 22, where a scatter plot between the modeled reaction rate using, either the independent β-PDF, copula approach or the DNN is compared to $\overline{\dot{\omega}}_{c_T}^{m-DNS}$. It is clearly seen that

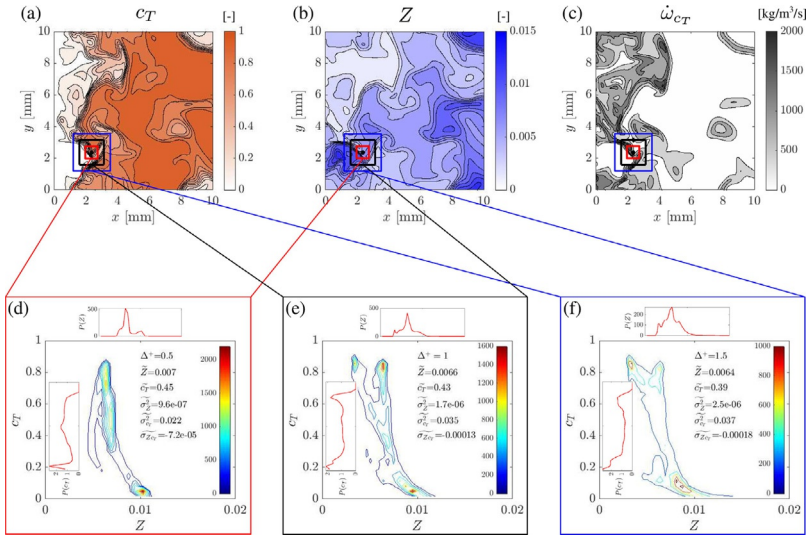

FIG. 17 Case AZ1: typical instantaneous x-y plane contours of unfiltered fields for (A) c_T, (B) Z, and (C) $\dot{\omega}_{c_T}$; and subgrid PDFs with three different filter sizes, (D) $\Delta^+ = 0.5$, (E) 1, and (F) 1.5, at an arbitrarily chosen point. *Adapted from Z.X. Chen, S. Iavarone, G. Ghiasi, V. Kanan, G. D'alessio, A. Parente, N. Swaminathan, Application of machine learning for filtered density function closure in MILD combustion, Combust. Flame 225 (2021) 160–179, https://doi.org/10.1016/j.combustflame.2020.10.043.*

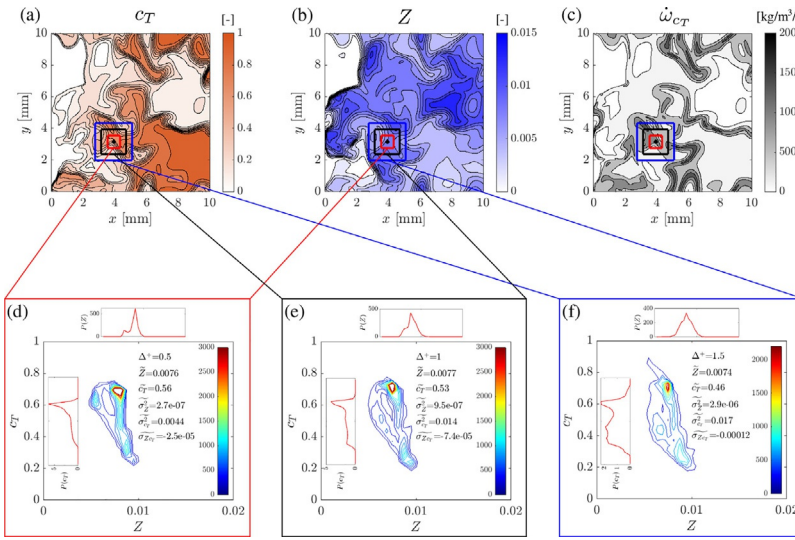

FIG. 18 Case AZ2: typical instantaneous x-y plane contours of unfiltered fields for (A) c_T, (B) Z, and (C) $\dot{\omega}_{c_T}$; and subgrid PDFs with three different filter sizes, (D) $\Delta^+ = 0.5$, (E) 1, and (F) 1.5, at an arbitrarily chosen point. *Adapted from Z.X. Chen, S. Iavarone, G. Ghiasi, V. Kanan, G. D'alessio, A. Parente, N. Swaminathan, Application of machine learning for filtered density function closure in MILD combustion, Combust. Flame 225 (2021) 160–179, https://doi.org/10.1016/j.combustflame.2020.10.043.*

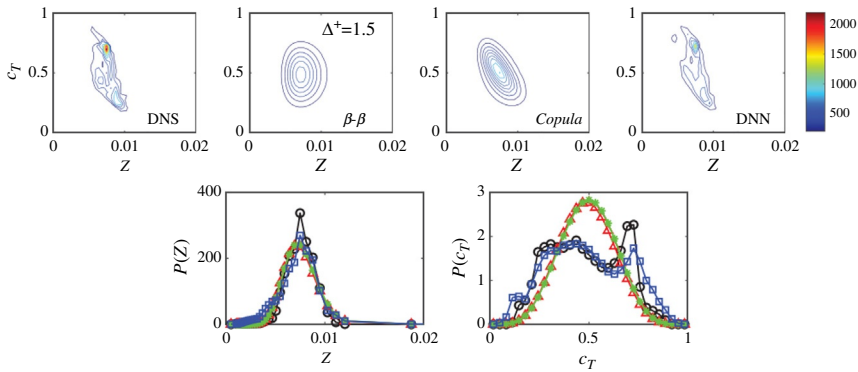

FIG. 19 Comparison of (*top*) joint and (*bottom*) marginal PDFs between DNS and model predictions for filter sizes of $\Delta^+ = 1.5$ for the filter point shown in Fig. 18. *Adapted from Z.X. Chen, S. Iavarone, G. Ghiasi, V. Kanan, G. D'alessio, A. Parente, N. Swaminathan, Application of machine learning for filtered density function closure in MILD combustion, Combust. Flame 225 (2021) 160–179, https://doi.org/10.1016/j.combustflame.2020.10.043.*

the DNN-based approach outperforms the β and copula model with a scatter much closer to the diagonal line.

4.2 Partially stirred reactor approach

Another modeling approach that has been assessed using the DNS data of nonpremixed MILD combustion with internal EGR discussed in Section 2.2 of Doan et al. [20] is the partially stirred reactor (PaSR) approach described by Iavarone et al. [45]. In this model historically introduced in Chomiak [46], each computational cell is split into a reacting region and a nonreacting region. The mean reaction rate in a specific cell is obtained based on a mass exchange between the two regions and expressed as

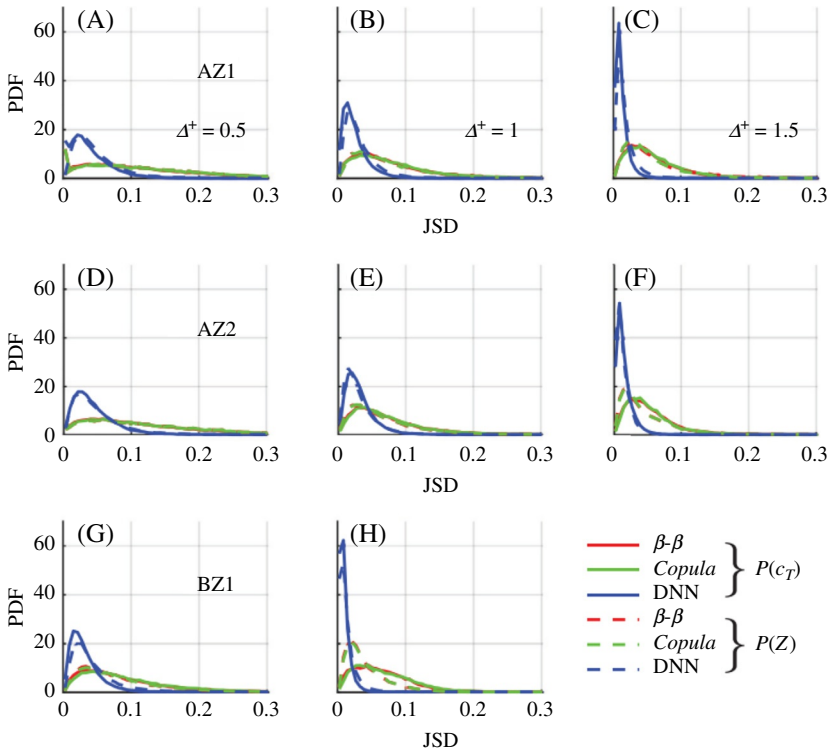

FIG. 20 PDF of Jansen-Shannon divergence (JSD) for DNS and modeled PDFs. *Solid and* dashed *lines* correspond to progress variable and mixture fraction, respectively. (A) to (C): case AZ1; (D) to (F): case AZ2; (G) to (H): case BZ1. (A)-(D)-(G): $\Delta^+ = 0.5$; (B)-(E)-(H): $\Delta^+ = 1$;(C)-(F): $\Delta^+ = 1.5$. *Adapted from Z.X. Chen, S. Iavarone, G. Ghiasi, V. Kanan, G. D'alessio, A. Parente, N. Swaminathan, Application of machine learning for filtered density function closure in MILD combustion, Combust. Flame 225 (2021) 160–179, https://doi.org/10.1016/j.combustflame.2020.10.043.*

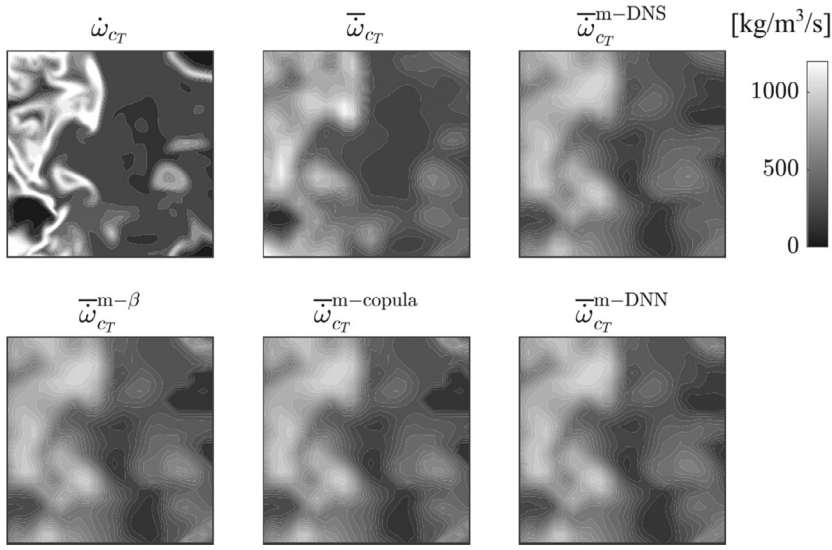

FIG. 21 Typical reaction rate contours for case AZ1 with $\Delta^+ = 0.5$. Mean flow moves from left to right. *Adapted from Z.X. Chen, S. Iavarone, G. Ghiasi, V. Kanan, G. D'alessio, A. Parente, N. Swaminathan, Application of machine learning for filtered density function closure in MILD combustion, Combust. Flame 225 (2021) 160–179, https://doi.org/10.1016/j.combustflame.2020.10.043.*

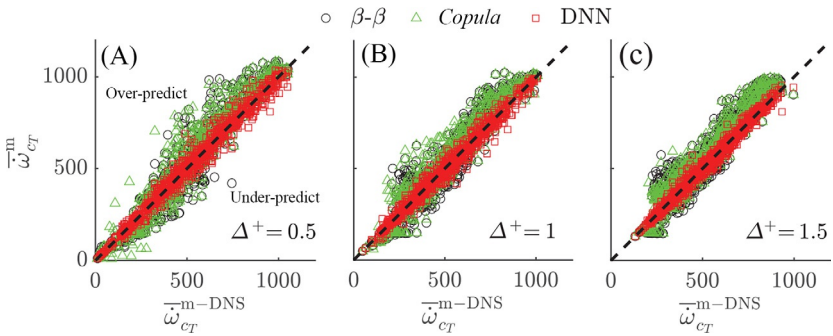

FIG. 22 Scatter plot of $\overline{\dot{\omega}}^{m-DNS}_{c_T}$ and $\overline{\dot{\omega}}^{m}_{c_T}$ (in units of kg/m^{-3} per s) modeled using different FDF models (denoted using different markers) for case AZ1 with different filter sizes. (A) $\Delta^+ = 0.5$; (B) $\Delta^+ = 1$; (C) $\Delta^+ = =1.5$.

$$\bar{\dot{\omega}}_\alpha = \kappa \frac{\overline{\rho}(Y^*_\alpha - Y^0_\alpha)}{\tau^*} \tag{15}$$

where Y^*_i and Y^0_i are the αth species mass fraction in the reacting and nonreacting regions, respectively, and τ^* is the residence time in the reacting region. κ is the volume fraction of the reacting region, which provides the

partially stirred nature of this model. In general, κ is estimated as the ratio between a chemical timescale τ_c and a mixing timescale τ_{mix}:

$$\kappa = \frac{\tau_c}{\tau_c + \tau_{mix}} \tag{16}$$

In addition, the species mass fraction in the reacting region is estimated from the evolution of an ideal reactor that evolves from Y_i^0 over a residence time τ^*, following the evolution equation:

$$\frac{dY_\alpha^*}{dt} = \frac{\dot{\omega}_\alpha^*}{\rho} \tag{17}$$

From the modeling equations presented earlier, it can be seen that the complexity in this model is inappropriately modeling τ^*, τ_c, and τ_{mix}. Various choices are possible and are discussed in [45, 47–49]. In particular, Iavarone et al. [45] analyzed different modeling approaches for τ_c and τ_{mix}, summarized in Table 6. Regarding τ^*, it is generally taken as equal to τ_{mix} [48] but can also be taken as the minimum between τ_{mix} and τ_c [47, 49]. This latter approach was the one chosen by Iavarone et al. [45].

From the modeling frameworks analyzed, it was observed that the best agreement between the filtered DNS heat release rate and modeled reaction rate was obtained when using the local dynamic approach for the estimation of $\tau_{mix} = \frac{\widetilde{\sigma_Z^2}}{\tilde{\xi}}$ in conjunction with $\tau_c = \max\left(\frac{Y_\alpha^*}{|dY_\alpha^*/dt|}\right)$. In addition, it was observed that, generally, $\tau_{mix} \ll \tau_c$. Therefore, τ_{mix} was the main driver in the accuracy of the modeling framework. However, the PaSR approach could only predict accurately the reaction rate of major species and showed significant overestimation for the modeling of the reaction rate of OH as is shown in Fig. 23. The region associated with this mismatch is located in a low heat releasing region in the downstream part of the domain. In those area, due to the nearly fully mixed mixture, τ_{mix} reaches very small values that lead to an overestimation of $\overline{\dot{\omega}}_\alpha$.

4.3 Flamelet-generated manifold

A final modeling approach which was tested based on DNS data is the FGM approach. In this modeling framework, it is assumed that there exists a lower dimension manifold in the composition space and that a

TABLE 6 Modeling equations for the PaSR approach.

τ_c	$\max\left(\frac{-\dot{\omega}_F}{Y_f}, \frac{-\dot{\omega}_O}{Y_O}\right)^{-1}$	$\max\left(\frac{Y_\alpha^*}{\lvert dY_\alpha^*/dt\rvert}\right)$	
τ_{mix}	$C_{mix}\frac{k}{\epsilon}$	$\sqrt{\frac{k}{\epsilon}\left(\frac{\mu}{\epsilon}\right)^{1/2}}$	$\frac{\widetilde{\sigma_Z^2}}{\tilde{\xi}}$

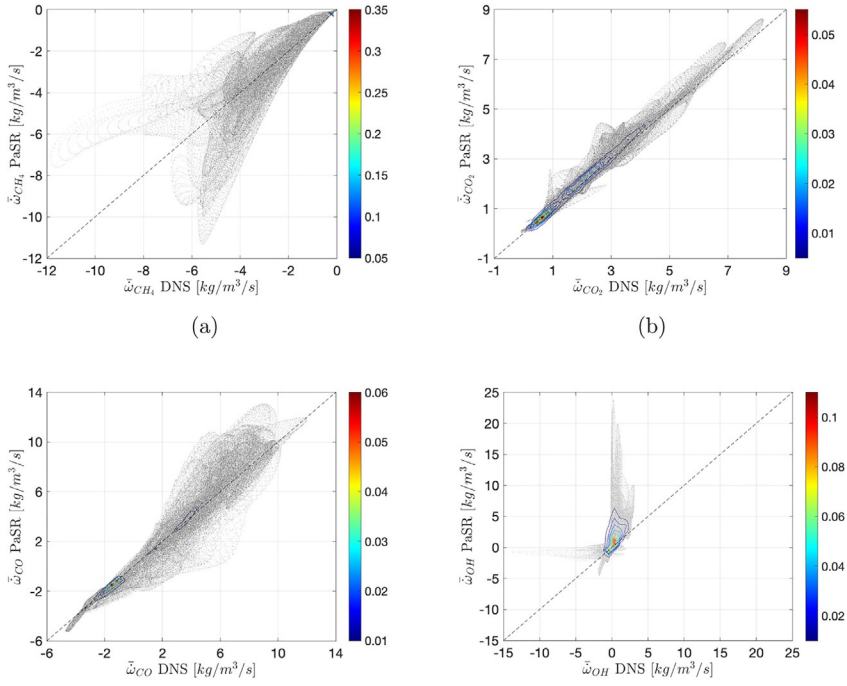

FIG. 23 Parity plots and contours of the joint PDF of the filtered chemical source terms $\overline{\omega}$ extracted from DNS and estimated by the PaSR model for: (A) CH_4, (B) CO_2, (C) CO, (D) OH. *Adapted from S. Iavarone, A. Péquin, Z.X. Chen, N.A.K. Doan, N. Swaminathan, A. Parente, An a priori assessment of the Partially Stirred Reactor (PaSR) model for MILD combustion, Proc. Combust. Inst. (2021), https://doi.org/10.1016/j.proci.2020.06.234 (in press).*

turbulent flame is an ensemble of 1D laminar flamelets [50]. As a result of those assumptions, a set of suitable 1D flames can be computed and solved prior to the turbulent simulation and all the thermochemical variables can be stored in look-up tables according to a few control variables (CV), which represent the manifold. Typical CVs are, for example, the reaction progress variable, c, or the mixture fraction, Z. The difficulty of using this modeling framework for MILD combustion originates from the coexistence of ignition and deflagration combustion modes as discussed in Section 3.3. As a result, there is no appropriate CV that can accurately describe the reaction rate evolution in both combustion modes. This observation served as a basis for the introduction of the multistage FGM proposed by Göktolga et al. [27].

In this work, two progress variables were used to describe the state of reaction (in addition to mixture fraction): the first one, noted $\mathcal{Y}_1$, based on

HO_2 that accurately describes the autoignition phase and the second one, noted $\mathcal{Y}_2$, based on H_2O which describes the subsequent ignition-oxidation phase. Using these two progress variables, two thermochemical tables can be constructed: one which spans the initial process (from the initial mixture until HO_2 reaches its maximum value) and a second table that starts from that mixture state until the end of the reaction. Those two progress variables are transported within the modeling framework, and depending on the value of the progress variable based on HO_2, the thermochemical quantities are either taken from the first or second table. These thermochemical tables were based on an igniting mixing layer (IML) [51]. This approach was tested a posteriori in a 2D DNS configuration similar to the 3D igniting mixing layer discussed in Section 2.1 from Göktolga et al. [18]. The obtained averaged reaction rates are shown in Fig. 24, where the better agreement of the multistage FGM approach can be observed compared to a conventional FGM based on a single progress variable.

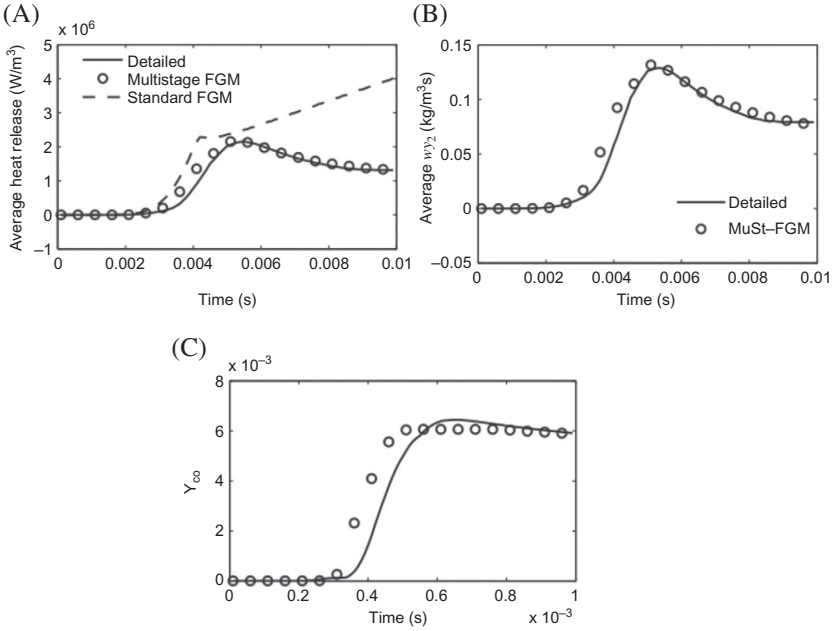

FIG. 24 Comparison of (A) the average heat release rate in W/m^3, (B) $\dot{\omega}_{\mathcal{Y}_2}$, and (C) $Y_{CO,max}$ between the multistage FGM and the average from the 2D DNS. *Adapted from M.U. Göktolga, J.A. van Oijen, L.P.H. de Goey, Modeling MILD combustion using a novel multistage FGM method, Proc. Combust. Inst. 36 (2017) 4269–4277, https://doi.org/10.1016/j.proci.2016.06.004.*

4.4 Discussion

From the modeling discussion in the previous sections, several common observations can be made. First, all these modeling frameworks relied mostly on ignition-based canonical laminar configurations, such as the PSR in Section 4.1, the PaSR in Section 4.2, or the igniting mixing layer in Section 4.3. This choice was supported by the observations on balance between ignition and deflagration presented in Section 3.3, where ignition was found to be the dominant mode of combustion in MILD combustion. However, these modeling frameworks had to include additional features to deal with the complex nature of MILD combustion. In the presumed PDF approach, this was done through the development of a machine-learning-based model for the subgrid PDF to account for the unique shape of the subgrid PDF that is the result of combined deflagrative and autoignition features. In the FGM approach, to account for this combined ignition/deflagration, two progress variables were introduced to deal with these two stages present in MILD combustion.

Those results highlight the complexity of modeling MILD combustion because it presents a variety of combustion modes. Therefore, conventional combustion model may generally fail at accurately reproducing the reaction rates in MILD combustion and additional research and more refined models are necessary.

5 Conclusions and outlook

In this chapter, findings and insights obtained from DNS of MILD combustion by various research groups have been discussed. These DNS cover a variety of configurations that can be encountered in MILD combustion apparatus: an autoigniting mixing layer with hot and diluted oxidizer [18], a premixed MILD mixture with internal EGR [22], and a nonpremixed MILD mixture with internal EGR [20]. The particular thermochemical and turbulent conditions of these DNS were discussed and while they do not reach the same turbulence levels as those in real experimental configurations due to the limit in computational resources, they still reach levels that can be representative of the conditions encountered in MILD combustion experiments, in terms of Reynolds and Karlovitz numbers. Therefore, these DNS provided a large number of insights into the physics of MILD combustion, which have been discussed.

Specifically, the inception of MILD combustion and its differences with conventional combustion were discussed, with the importance of radicals and continuous autoignition highlighted. In addition, evidence of the coexistence of ignition and deflagration were discussed, as well as the prominence of autoignition in the total heat release rate. These

considerations, obtained from DNS, were then contrasted with existing modeling frameworks for MILD combustion, and models which accounted for these particularities of MILD combustion were shown to perform better.

While all the work discussed in this chapter provided a significant understanding of the inception of MILD combustion and the balance between the different combustion modes that could be used as a basis to develop models, there remain many aspects that still need to be researched. Specifically, the modeling frameworks discussed earlier have mostly only been tested in a priori settings. To properly assess their accuracy, they also have to be tested a posteriori in LES and RANS simulations. In addition, the DNS discussed here has a limited range of turbulence and thermochemical conditions, and it would therefore be of interest to perform DNS in a more representative range, closer to the one that can be encountered in experiments. That would allow determining whether the observations highlighted here are still valid for those conditions or whether the physics of MILD combustion changes. Finally, while most of the heat release rate originated from autoigniting structures, developing a model which can selectively switch combustion modes could allow for even better accuracy with research relying on data-driven approaches currently exploring that possibility [52].

References

[1] J.A. Wünning, Flameless oxidation with highly preheated air, Chem. Ing. Tech. 63 (1991) 1243–1245.

[2] J.A. Wünning, J.G. Wünning, Flameless oxidation to reduce thermal no-formation, Prog. Energy Combust. Sci. 23 (1) (1997) 81–94, https://doi.org/10.1016/S0360-1285(97)00006-3.

[3] A. Cavaliere, M de Joannon, Mild combustion, Prog. Energy Combust. Sci. 30 (4) (2004) 329–366, https://doi.org/10.1016/j.pecs.2004.02.003.

[4] A.A.V. Perpignan, A. Gangoli Rao, D.J.E.M. Roekaerts, Flameless combustion and its potential towards gas turbines, Prog. Energy Combust. Sci. 69 (2018) 28–62, https://doi.org/10.1016/j.pecs.2018.06.002.

[5] M. Katsuki, T. Hasegawa, The science and technology of combustion in highly preheated air, 27th Symp. (Int.) Combust. 27 (1998) 3135–3146, https://doi.org/10.1016/S0082-0784(98)80176-8.

[6] I.B. Ozdemir, N. Peters, Characteristics of the reaction zone in a combustor operating at MILD combustion, Exp. Fluids 30 (6) (2001) 683–695, https://doi.org/10.1007/s003480000248.

[7] T. Plessing, N. Peters, J.G. Wünning, Laseroptical investigation of highly preheated combustion with strong exhaust gas recirculation, 27th Symp. (Int.) Combust. 27 (1998) 3197–3204, https://doi.org/10.1016/S0082-0784(98)80183-5.

[8] B.B. Dally, A.N. Karpetis, R.S. Barlow, Structure of turbulent non-premixed jet flames in a diluted hot coflow, Proc. Combust. Inst. 29 (x) (2002) 1147–1154, https://doi.org/10.1016/S1540-7489(02)80145-6.

[9] C. Duwig, B. Li, Z.S. Li, M. Aldén, High resolution imaging of flameless and distributed turbulent combustion, Combust. Flame 159 (1) (2012) 306–316, https://doi.org/10.1016/j.combustflame.2011.06.018.
[10] B.B. Dally, E. Riesmeier, N. Peters, Effect of fuel mixture on moderate and intense low oxygen dilution combustion, Combust. Flame 137 (4) (2004) 418–431, https://doi.org/10.1016/j.combustflame.2004.02.011.
[11] E. Oldenhof, M.J. Tummers, E.H. van Veen, D.J.E.M. Roekaerts, Ignition kernel formation and lift-off behaviour of jet-in-hot-coflow flames, Combust. Flame 157 (6) (2010) 1167–1178, https://doi.org/10.1016/j.combustflame.2010.01.002.
[12] P.R. Medwell, P.A.M. Kalt, B.B. Dally, Simultaneous imaging of OH, formaldehyde, and temperature of turbulent nonpremixed jet flames in a heated and diluted coflow, Combust. Flame 148 (1–2) (2007) 48–61, https://doi.org/10.1016/j.combustflame.2006.10.002.
[13] M de Joannon, A. Saponaro, A. Cavaliere, Zero-dimensional analysis of diluted oxidation of methane in rich conditions, Proc. Combust. Inst. 28 (2) (2000) 1639–1646, https://doi.org/10.1016/S0082-0784(00)80562-7.
[14] J.A.M. Sidey, E. Mastorakos, Visualization of MILD combustion from jets in cross-flow, Proc. Combust. Inst. 35 (3) (2015) 3537–3545, https://doi.org/10.1016/j.proci.2014.07.028.
[15] P.R. Medwell, P.A.M. Kalt, B.B. Dally, Imaging of diluted turbulent ethylene flames stabilized on a Jet in Hot Coflow (JHC) burner, Combust. Flame 152 (1–2) (2008) 100–113, https://doi.org/10.1016/j.combustflame.2007.09.003.
[16] E. Abtahizadeh, A.V. Sepman, F. Hernández-Pérez, J.A. van Oijen, A.V. Mokhov, L.P.H de Goey, H.B. Levinsky, Numerical and experimental investigations on the influence of preheating and dilution on transition of laminar coflow diffusion flames to mild combustion regime, Combust. Flame 160 (11) (2013) 2359–2374, https://doi.org/10.1016/j.combustflame.2013.05.020.
[17] E. Mastorakos, Ignition of turbulent non-premixed flames, Prog. Energy Combust. Sci. 35 (1) (2009) 57–97, https://doi.org/10.1016/j.pecs.2008.07.002.
[18] M.U. Göktolga, J.A. van Oijen, L.P.H de Goey, 3D DNS of MILD combustion: a detailed analysis of heat loss effects, preferential diffusion, and flame formation mechanisms, Fuel 159 (2015) 784–795, https://doi.org/10.1016/j.fuel.2015.07.049.
[19] Y. Minamoto, T.D. Dunstan, N. Swaminathan, R.S. Cant, DNS of EGR-type turbulent flame in MILD condition, Proc. Combust. Inst. 34 (2) (2013) 3231–3238, https://doi.org/10.1016/j.proci.2012.06.041.
[20] N.A.K. Doan, N. Swaminathan, Y. Minamoto, DNS of MILD combustion with mixture fraction variations, Combust. Flame 189 (2018) 173–189, https://doi.org/10.1016/j.combustflame.2017.10.030.
[21] A. Kazakov, M. Frenklach, DRM19, http://www.me.berkeley.edu/drm/ (last accessed: 24 May 2022).
[22] Y. Minamoto, N. Swaminathan, R.S. Cant, T. Leung, Reaction zones and their structure in MILD combustion, Combust. Sci. Technol. 186 (8) (2014) 1075–1096, https://doi.org/10.1080/00102202.2014.902814.
[23] M.D. Smooke, V. Giovangigli, M.D. Smooke, V. Giovangigli, Formulation of the premixed and nonpremixed test problems, in: M.D. Smooke (Ed.), Reduced Kinetic Mechanisms and Asymptotic Approximations for Methane-Air Flames, Lecture Notes in Physics, 384, Springer, Berlin, Heidelberg, 1991, pp. 1–28, https://doi.org/10.1007/bfb0035363. vol.
[24] T. Poinsot, Boundary conditions for direct simulations of compressible viscous flows, J. Comput. Phys. 101 (1992) 104–129, https://doi.org/10.1016/0021-9991(92)90227-P.
[25] Y. Minamoto, N. Swaminathan, R.S. Cant, T. Leung, Morphological and statistical features of reaction zones in MILD and premixed combustion, Combust. Flame 161 (11) (2014) 2801–2814, https://doi.org/10.1016/j.combustflame.2014.04.018.

[26] N. Peters, Turbulent Combustion, Cambridge University Press, Cambridge, 2000.
[27] M.U. Göktolga, J.A. van Oijen, L.P.H de Goey, Modeling MILD combustion using a novel multistage FGM method, Proc. Combust. Inst. 36 (2017) 4269–4277, https://doi.org/10.1016/j.proci.2016.06.004.
[28] Y. Minamoto, N. Swaminathan, Modelling paradigms for MILD combustion, Int. J. Adv. Eng. Sci. Appl. Math. 6 (1–2) (2014) 65–75, https://doi.org/10.1007/s12572-014-0106-x.
[29] Y. Minamoto, N. Swaminathan, Subgrid scale modelling for MILD combustion, Proc. Combust. Inst. 35 (3) (2015) 3529–3536, https://doi.org/10.1016/j.proci.2014.07.025.
[30] N.A.K. Doan, N. Swaminathan, Autoignition and flame propagation in non-premixed MILD combustion, Combust. Flame 201 (2019) 234–243, https://doi.org/10.1016/j.combustflame.2018.12.025.
[31] N.A.K. Doan, N. Swaminathan, Role of radicals on MILD combustion inception, Proc. Combust. Inst. 37 (4) (2019) 4539–4546, https://doi.org/10.1016/j.proci.2018.07.038.
[32] N.A.K. Doan, S. Bansude, K. Osawa, Y. Minamoto, T. Lu, J.H. Chen, N. Swaminathan, Identification of combustion mode under MILD conditions using chemical explosive mode analysis, Proc. Combust. Inst. (2021), https://doi.org/10.1016/j.proci.2020.06.293.
[33] T. Echekki, J.H. Chen, Direct numerical simulation of autoignition in non-homogeneous hydrogen-air mixtures, Combust. Flame 134 (3) (2003) 169–191.
[34] C.S. Yoo, R. Sankaran, J.H. Chen, Three-dimensional direct numerical simulation of a turbulent lifted hydrogen jet flame in heated coflow: flame stabilization and structure, J. Fluid Mech. 640 (2009) 453–481.
[35] C.S. Yoo, E.S. Richardson, R. Sankaran, J.H. Chen, A DNS study on the stabilization mechanism of a turbulent lifted ethylene jet flame in highly-heated coflow, Proc. Combust. Inst. 33 (1) (2011) 1619–1627, https://doi.org/10.1016/j.proci.2010.06.147.
[36] T.F. Lu, C.S. Yoo, J.H. Chen, C.K. Law, Three-dimensional direct numerical simulation of a turbulent lifted hydrogen jet flame in heated coflow: a chemical explosive mode analysis, J. Fluid Mech. 652 (2010) 45–64, https://doi.org/10.1017/S002211201000039X.
[37] C. Xu, J.W. Park, C.S. Yoo, J.H. Chen, T. Lu, Identification of premixed flame propagation modes using chemical explosive mode analysis, Proc. Combust. Inst. 37 (2) (2019) 2407–2415, https://doi.org/10.1016/j.proci.2018.07.069.
[38] K. Aditya, A. Gruber, C. Xu, T. Lu, A. Krisman, M.R. Bothien, J.H. Chen, Direct numerical simulation of flame stabilization assisted by autoignition in a reheat gas turbine combustor, Proc. Combust. Inst. 37 (2) (2019) 2635–2642, https://doi.org/10.1016/j.proci.2018.06.084.
[39] C. Xu, A.Y. Poludnenko, X. Zhao, H. Wang, T. Lu, Structure of strongly turbulent premixed n-dodecane-air flames: direct numerical simulations and chemical explosive mode analysis, Combust. Flame 209 (2019) 27–40, https://doi.org/10.1016/j.combustflame.2019.07.027.
[40] M.B. Luong, G.H. Yu, S.H. Chung, C.S. Yoo, Ignition of a lean PRF/air mixture under RCCI/SCCI conditions: a comparative DNS study, Proc. Combust. Inst. 36 (3) (2017) 3623–3631, https://doi.org/10.1016/j.proci.2016.08.038.
[41] J.H. Chen, E.R. Hawkes, R. Sankaran, S.D. Mason, H.G. Im, Direct numerical simulation of ignition front propagation in a constant volume with temperature inhomogeneities I. Fundamental analysis and diagnostics, Combust. Flame 145 (2006) 128–144, https://doi.org/10.1016/j.combustflame.2005.09.017.
[42] Z.X. Chen, S. Iavarone, G. Ghiasi, V. Kanan, G. D'alessio, A. Parente, N. Swaminathan, Application of machine learning for filtered density function closure in MILD combustion, Combust. Flame 225 (2021) 160–179, https://doi.org/10.1016/j.combustflame.2020.10.043.
[43] O.R. Darbyshire, N. Swaminathan, A presumed joint PDF model for turbulent combustion with varying equivalence ratio, Combust. Sci. Technol. 184 (12) (2012) 2036–2067, https://doi.org/10.1080/00102202.2012.696566.

[44] R.L. Plackett, A class of bivariate distributions, J. Am. Stat. Assoc. 60 (310) (1965) 516–522.
[45] S. Iavarone, A. Péquin, Z.X. Chen, N.A.K. Doan, N. Swaminathan, A. Parente, An a priori assessment of the Partially Stirred Reactor (PaSR) model for MILD combustion, Proc. Combust. Inst. (2021), https://doi.org/10.1016/j.proci.2020.06.234. in press.
[46] J. Chomiak, Combustion: A Study in Theory, Fact and Application, Abacus Press/Gordon and Breach Science Publishers, New York, 1990.
[47] S. Iavarone, M. Cafiero, M. Ferratrotti, F. Contino, A. Parente, A multiscale combustion model formulation for NO_x predictions in hydrogen enriched jet flames, Int. J. Hydrog. Energy 44 (41) (2019) 23436–23457.
[48] N. Nordin, Complex Chemistry Modeling of Diesel Spray Combustion (Ph.D. thesis), Chalmers University of Technology, 2001.
[49] M. Ferrarotti, M. Furst, E. Cresci, W de Paepe, A. Parente, Key modeling aspects in the simulation of a quasi-industrial 20 kW moderate or intense low-oxygen dilution combustion chamber, Energy Fuels 32 (10) (2018) 10228–10241.
[50] N. Peters, Laminar diffusion flamelet models in non-premixed turbulent combustion, Prog. Energy Combust. Sci. 10 (1984) 319–339.
[51] E. Abtahizadeh, L.P.H de Goey, J.A. van Oijen, Development of a novel flamelet-based model to include preferential diffusion effects in autoignition of CH4/H2 flames, Combust. Flame 162 (11) (2015) 4358–4369, https://doi.org/10.1016/j.combustflame.2015.06.015.
[52] K. Jigjid, C. Tamaoki, Y. Minamoto, R. Nakazawa, N. Inoue, M. Tanahashi, Data driven analysis and prediction of MILD combustion mode, Combust. Flame 223 (2021) 474–485, https://doi.org/10.1016/j.combustflame.2020.10.025.